IOPscience iopscience.iop.org

Home Search Collections Journals About Contact us My IOPscience

Electron interferometry and interference electron microscopy

This content has been downloaded from IOPscience. Please scroll down to see the full text.

1981 J. Phys. E: Sci. Instrum. 14 649

(http://iopscience.iop.org/0022-3735/14/6/001)

View the table of contents for this issue, or go to the journal homepage for more

Download details:

IP Address: 130.92.9.55
This content was downloaded on 05/09/2014 at 14:38

Please note that terms and conditions apply.

J. Phys. E: Sci. Instrum., Vol. 14, 1981. Printed in Great Britain

**REVIEW ARTICLE**

# Electron interferometry and interference electron microscopy

**G F Missiroli, G Pozzi and U Valdrè**
Istituto di Fisica and GNSM–CNR, University of Bologna, Via Irnerio 46, 40126 Bologna, Italy

**Abstract** A state-of-the-art review of electron interferometry and interference electron microscopy is given. The various types of interferometry device, interferometers and interference microscopes, which have been proposed and/or constructed are reviewed and commented upon. The electron biprism, by far the most successful interferometry device, is treated in some detail from both the experimental and theoretical (geometric and wave optics) points of view. The applications of electron interferometry are presented with particular reference to off-axis electron holography. Finally the future perspectives are indicated.

## 1 Introduction

Electron interferometry is defined here as that branch of electron optics dealing with interference phenomena produced with the aid of suitable devices under instrumental and specimen conditions controlled by the experimenter. Its origin dates back to 1953 when the first interference pattern was obtained (Marton *et al* 1953), but it was only with the introduction of the electrostatic biprism and with the assessment that the coherence of the electron wave is preserved when it passes through a thin specimen that electron interferometry was established as a practical proposition (Möllenstedt and Düker 1956, Möllenstedt and Keller 1957, Faget and Fert 1957a, b). Since then work has been carried out more or less erratically except in a very few laboratories.

There has recently been a revival in the applications of electron interferometry and further development is expected in view of the availability of field emission sources, which have reasonably good stability, high brightness and high coherence. It is therefore felt that a review of the subject would be appropriate and timely.

There have been several reviews of interferometry which have concentrated on the efforts of certain groups or institutions: Faget and Fert (1957b), Faget (1961) and Fert (1961, 1962) refer especially to work carried out in the Laboratoire d'Optique Electronique at Toulouse in a discussion of the general background, the instrumentation and applications while Möllenstedt (1960), Möllenstedt and Lenz (1962) and Wahl (1970c) have given brief reports on activity at the University of Tübingen; a more recent summary of this work has been given by Möllenstedt and Lichte (1979). Also, Hibi and Yada (1976) have given a review of some of the literature up to 1973, with special emphasis on the contribution of Japanese workers to this field. However, an up-dated, impartial and comprehensive review is not available, and it is one of the aims of the present article to fill this gap.

As the nomenclature of electron interferometry instrumentation is still the reserve of specialists and often reflects personal taste, a few definitions are given here (and, when required, in the following pages), in order to avoid misunderstanding. The device used to produce two or more coherent waves, essential for the occurrence of interference, will be called an *interferometry device*. The instrument used to perform interferometry with no imaging facilities for the specimen will be designated an *electron interferometer*. This is usually an electron optical bench, capable of great electrical and mechanical flexibility, in particular for specimen preparation, treatment and handling. Since the specimen is out of focus, only simple types of specimen of known geometry can be used. The name (electron) *interference microscope* refers to a machine where it is possible to obtain an interference pattern by coherently superimposing different regions of a focused (or nearly focused) image of the specimen. This instrument is usually a conventional electron microscope equipped with an interferometry device and capable of forming an image of the specimen, in addition to displaying the interference pattern.

In the following, the applications, capability and future perspectives of electron interferometry and interference electron microscopy will be presented and discussed. Section 2 contains a critical review of the various interferometry devices developed so far and is followed by §§3 and 4, respectively covering the theoretical and practical features of the biprism, by far the most successful device, while §5 deals with applications of electron interferometers and electron interference microscopes.

## 2 Types of interferometry device

This section will review the basic ideas and the various types of interferometry device prompted by them and will also make a critical appraisal of their performance and fields of application.

The close similarity between light optics and electron optics is used to classify interferometry devices into two categories: (i) division of amplitude (e.g. Michelson's interferometer in light optics) and (ii) division of wavefront (e.g. Fresnel biprism). It will be seen that the electrostatic biprism, which belongs to the second category, is by far the most popular device in electron optics, although, significantly, the other category is more popular in light optics.

0022-3735/81/060649+23 $01.50 © 1981 The Institute of Physics

2.1 *Division of amplitude*

2.1.1 *Three-crystal interferometry device.* Historically, the first interferometry device to be conceived (Marton 1952) and actually built (Marton *et al* 1953, 1954, Marton 1954) was in some ways the equivalent of the optical interferometer of Mach and Zehnder. It is based on the initial splitting (e.g. rays 1 and 2 in figure 1), produced through Bragg reflection by a single crystal film $C_1$, of a fairly coherent electron beam I, on the further splitting (i.e., Bragg reflection, e.g. rays 3 and 4) produced by a second crystal $C_2$, and on the recombination (emerging ray E) caused by a third crystal $C_3$, again by Bragg reflection. The three crystals must satisfy several stringent requirements, namely they must have the same crystal structure and must be flat, parallel to each other and of the same orientation and register. The required geometry is obtained by providing a suitable support which allows movement along, and rotation around, the optical axis ($z$) for the first crystal $C_1$, $z$ rotation for $C_2$ and $z$ rotation and tilt for $C_3$.

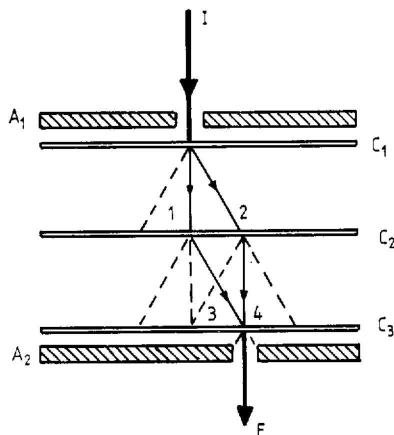


**Figure 1** Schematic representation of a Marton-type amplitude splitting electron interferometry device. I, incident beam; $C_1$, $C_2$, $C_3$, thin single crystals of identical material and orientation, accurately aligned; $A_1$, $A_2$, beam limiting apertures; E, exit beam formed by two interfering Bragg-diffracted beams.

A set of interference fringes is obtained on a photographic plate, placed in a plane which is conjugate, through a lens, with the exit surface of the third crystal. The lens is necessary in order to suitably magnify the fringe pattern; apertures $A_1$ and $A_2$ must be used in order to avoid the presence of unwanted beams. If an object is interposed in the path of ray 1 or 2, the set of fringes is altered (see §§3.1.2 and 5.1).

The distance between two consecutive copper crystals grown epitaxially to a thickness of 10 nm was 35 mm, bringing the maximum separation of the split beams 1 and 2 to 0.7 mm. The Cu films were 3 mm in diameter and the accelerating voltage was 60 kV. Over 1200 micrographs had to be taken, each with an exposure time exceeding 6 min, in order to establish beyond any doubt the occurrence of interference fringes.

An elementary theory of the three-crystal interferometry device was developed by Simpson (1954) and good correlation was found with experimental data.

It is clear that this method suffers from various inconveniences: (i) difficult and crucial alignment of the three crystals; (ii) low intensity due to the various splittings of the incoming beam and also to absorption effects (in fact the alignment had to be performed by means of micrographs because the intensity of the fringes was below the threshold for their direct observation on the fluorescent screen); (iii) lack of versatility. An attempt to increase the intensity of the interference pattern (theoretically by two orders of magnitude) by replacing the second crystal with a lens also produced disappointing results (Simpson 1956), probably because of the aberrations introduced by the lens. For the above reasons the experiment has never been repeated, and its interest in electron microscopy is purely historical and academic.

The principle of this method was, however, applied successfully ten years later in x-ray and neutron interferometry, where the crystal requirements are less stringent than those for electron interferometry (for a review, see Bonse and Graeff 1977).

2.1.2 *Other methods.* Other interference methods, based on amplitude splitting by crystals, have been proposed or developed; all of them use convergent-beam techniques.

Li (1978) has proposed a modified version of the three-crystal Marton interferometer which is based on Fraunhofer diffraction rather than Fresnel diffraction. It should provide some advantages, but the basic criticism of the Marton interferometer still holds and, to our knowledge, experiments have never been attempted.

The formation of interference fringes, by overlapping thin crystals in convergent-beam electron microscopy, in both the central beam and the diffracted orders, has been described by Dowell and Goodman (1973) and interpreted by Dowell (1977). Similar results have been obtained from two suitably orientated thin crystals separated by a gap in convergent-beam electron diffraction patterns (Rackham *et al* 1977, Buxton *et al* 1978). In this case lattice parameters can be measured with an accuracy of 0.2% and it is claimed that double-crystal devices can be produced routinely by bombarding the edge of a crystal with ions until a gap is formed. Because of the small gap (10 μm wide at the most) between the crystals, the use of the system as a proper interferometry device is doubtful.

Interference effects in the Fraunhofer diffraction pattern have also been observed by Berndt and Doll (1978). They obtained the beam splitting by amplitude division with a diffraction grating of 1 μm spacing, placed in the condenser aperture plane; the (periodic) object was a replica grating of 0.463 μm spacing, placed in the normal specimen plane. The coherent superposition of neighbouring reflections in the diffraction plane can be used to determine the phase of structure factors, as first suggested by Hegerl and Hoppe (1970), who introduced the terminology of 'ptychography' for this method. They had in mind the use of an electrostatic biprism to obtain wavefront division (see §2.2.5), but no further attention was given to the subject; on the other hand, Berndt and Doll (1976, 1978) have proposed the use of amplitude division obtained by a grating and have analysed, both theoretically and experimentally by, first, light-optics simulation and, more recently, by electron optics, the feasibility of the method.

It should be noted in passing that lattice fringes are also formed by interference between the primary beam and the Bragg-reflected beam(s), as first observed by Menter (1956) (see also §5.8). Similarly, Fresnel fringes visible at the specimen edges are the result of interference between the direct beam proceeding through the vacuum and the beam scattered from the edge.

2.2 *Division of wavefront*

2.2.1 *Electrostatic biprism and related devices.* The electrostatic field, produced by a straight, charged wire W placed between two earthed plates, splits the wavefront of incoming

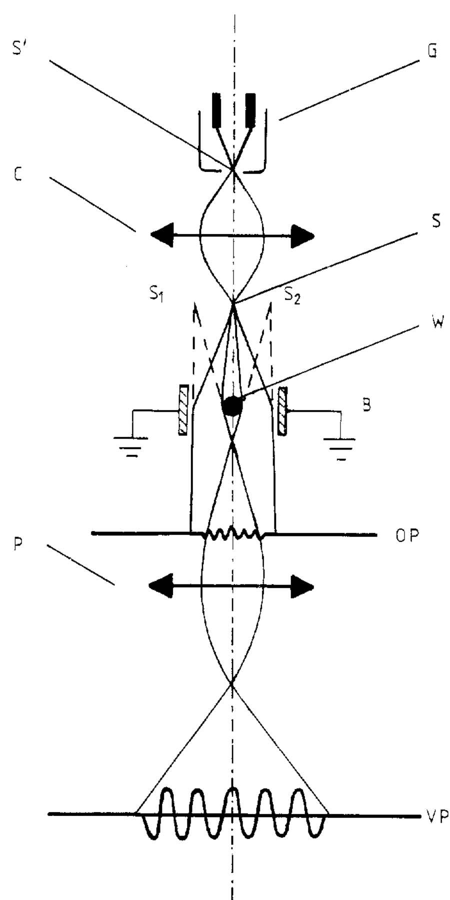


**Figure 2** Schematic electron ray path in an electron microscope equipped with a convergent biprism. G, electron gun; S′, primary electron source; C, condenser lens system; S, demagnified effective source; B, biprism; W, biprism wire; OP, observation plane; P, projector lens system; VP, final viewing plane conjugate to the observation plane.

electrons from the source S to produce two virtual, coherent electron sources $S_1$ and $S_2$ (figure 2; see also figure 5). Interference takes place in the region where the two split beams overlap. The principles of this method are analogous to those of the Fresnel biprism in light optics and this interferometry device is therefore called an electron biprism.

Figure 2 also shows diagrammatically the arrangement used by Möllenstedt and Düker (1955) in their early and successful work carried out in a conventional electron microscope of the electrostatic type. The cross-over S′ of the electron gun G is demagnified into the effective source S by the condenser system C in order to increase the lateral coherence of S, while a second lens system P below the biprism B is used to obtain a magnified image of the unlocalised fringe pattern present in the region of beam overlapping. This represents the type of arrangement commonly used in electron interferometry.

Let the observation plane OP, conjugate to the viewing screen VP (photographic plate), be below the biprism wire W and the effective source S be above the wire as depicted in figure 2. When no voltage is applied to the wire, its shadow is observed together with a system of diffraction fringes (see figure 6(*a*)). By increasing the positive voltage applied (convergent biprism), the shadow can be seen to shrink and a system of real interference fringes appears, if the coherence condition (equation (11), §§3.1.1 and 5.6) is satisfied (see figures 6(*b*) and (*c*). By applying a negative voltage (divergent biprism), the two electron beams in the region below the wire diverge and the width of the region not illuminated by the beam increases. A virtual interference field is produced above the wire; sections of this field can be imaged by a suitable excitation of lens system **P**.

It should be noted that in the case of a convergent biprism, the lens system P is used to form an enlarged image of the fringe pattern in the VP, while in the case of the divergent biprism, P has the additional, essential function of producing a real image of the virtual fringe system (§3.2.2).

One advantage of the biprism is that the fringe spacing can be varied over a wide range to suit the observation conditions, simply by changing the voltage applied to the wire (§3.1.1, equation (8)). Furthermore, there is no intensity splitting and, since the electron beam travels all the time in free space, unlike in the three-crystal method, the beam intensity is not reduced. However, impracticable exposure times were required even in such favourable conditions, so that Möllenstedt and Düker were forced to adopt electron optical devices of cylindrical symmetry (linear illumination and cylindrical lenses). With this approach they were able to observe, with the naked eye, interference fringes projected directly on to a fluorescent screen (Düker 1955, Möllenstedt and Düker 1956).

Since then the experimental conditions and the construction of the biprism have been improved, as we will see in §4. More details concerning the properties and the operation of the biprism will be given in §3. Interferometry devices which are based on the biprism will be outlined in §§2.2.1.1, 2.2.1.2, 2.2.4 and 2.2.5.

2.2.1.1 *Wire cascade biprisms.* Several wires at suitable potentials are placed one above the other. The aim is to increase the separation between the two split beams, without breaking the spatial coherence condition, in order to insert an object between them.

Möllenstedt and Bayh (1961) have described a system formed by three biprisms in cascade (at distances of 470 mm and 50 mm) to obtain both the separation of 60 $\mu$m required for experiments on the Aharonov–Bohm effect (§5.3) and a fringe system directly visible on the fluorescent screen.

The separation depends on the voltage applied to the first wire (divergent biprism) and on the distance between the first and second wires (convergent biprism).

However, as well as increasing the separation of the two interfering beams, the first two biprisms produce an increase in the distance between the two virtual sources so that the fringe system cannot be resolved directly on the fluorescent screen (§3.1.1, equation (8)). Hence the necessity of using a third wire (divergent biprism) to restore visibility.

In a modified version, Schaal *et al* (1966/7) have replaced the second biprism with an electrostatic lens to obtain a beam separation of up to 120 $\mu$m.

2.2.1.2 *Multiple beam devices.* Multiple beam interference has attracted the attention of some experimenters because it has, at least in theory, several advantages: (i) high sensitivity to phase changes, (ii) high intensity maxima ($N$-beam interference should produce maxima $\frac{1}{4}N^2$ times those of a two-beam pattern) and (iii) narrow maximum width. Buhl (1961a) was the first to use three-beam interferometry, while Anaskin and Stoyanova (1967, 1968d, e) and Anaskin *et al* (1968b) have performed more extensive experiments, using up to five beams, with a parallel array of biprisms obtained by mounting several wires on a hollow, optically polished support. In order to change the distance between the virtual electron sources (§3.1.1), the plane formed by the wires could be tilted with

respect to the optical axis of the electron microscope where the interferometry device was mounted. However, these devices suffer from several disadvantages: the parallelism of the wires is strictly stipulated, the device is sensitive both to irregularities and differences in the wire diameter, and to unequal voltage, and an accurate orientation of the wires with the optical axis is required in order to produce true $N$-beam interference.

The theoretical expectations of the performance of these devices have been confirmed satisfactorily. However, the finite size of the sources produces fringe intensities which are smaller than the calculated values; in the case of three-beam interference, the intensity with respect to the two-beam case is 1.4 instead of the theoretical value of $\frac{9}{4}=2.25$ (Anaskin and Stoyanova 1967).

2.2.1.3 *Charged film edge*. Interference patterns have been obtained near the edge of a charged thin film (placed between two earthed grids) as a result of the superposition of the beam transmitted through the specimen and of the beam travelling in free space near the film edge (Anaskin *et al* 1968a). This second beam is deflected by the electrostatic field created by the applied voltage. The experiments were performed in an electron microscope by suitable defocusing on thin (30–50 nm) carbon and collodion films. The interference pattern is visible near the edge of the film and, in the case of positively charged films, appears against the background of its low magnification shadow image (650 × ). The character of the fringe pattern is similar to that of a conventional biprism. The authors have suggested that this method could be applied in electron holography; however, the lack of control on the geometry of the edge may pose severe limitations.

Similar effects are produced by the electrostatic field created by charged specimens under beam irradiation.

2.2.2 *Magnetic biprisms*. A magnetic field is used to split the wavefront. This field may be produced by electromagnets (e.g. quadrupoles, Krimmel 1960) or by the inner magnetisation of a thin ferromagnetic film in the region where the direction of magnetisation changes (Boersch *et al* 1960, 1962b).

In the latter case the method has been used only to study the distribution of the magnetisation within the domain walls (for a recent review, see Jakubovics 1976). In fact, as an interferometry device, it suffers from inconveniences similar to those of the Marton interferometer: firstly, loss of intensity and coherence in the beam when passing through the magnetic material and, secondly, a lack of versatility.

The magnetic quadrupole is, on the contrary, free from the above disadvantages and also from the spurious effects introduced by the shadow of the wire in the biprism; furthermore it produces achromatic fringes. However, no applications have been reported in the literature, probably because the interpretation of the interference effects is very complicated (Krimmel 1961) and therefore it is difficult to separate these effects from those to be investigated in a specimen.

2.2.3 *Young interferometers*. Faget and Fert (1956, 1957b) were the first to show the occurrence of fringes from the interference of two electron waves transmitted by two circular holes (Young fringes). In order to obtain the required coherence with their thermo-ionic electron source, the beam was so defocused that the resulting intensity at the image plane was too low, the exposure times were too long and the disturbing effects were too great; in fact their results are not comparable with the calculated fringe pattern. The experiment has recently been repeated for the sake of completeness by Ohtsuki and Zeitler (1977) with the aid of a field emission source, and impressive results have been obtained.

In all the above experiments, it is the accidental occurrence of holes at a suitable distance in a carbon or gold film which provides the secondary sources. On the contrary, Möllenstedt and Jönsson (1959), Jönsson (1961) and Jönsson *et al* (1974) managed to prepare multiple (up to five) slits (50 $\mu$m long, 0.3 $\mu$m wide, with a spacing of 1 $\mu$m) in controlled conditions, and were able to produce Young fringes in agreement with the theory, to a first approximation. Deviations of the patterns from the theoretical predictions are attributed to the finite width of the slits. It should be emphasised that in this experiment, contrary to the light optics analogue, the coherent illumination of the slits could be an *a priori* problem. In fact, the dimensions of the slits are over $10^6$ times greater than the electron wavelength (see also §5.6), while in light optics the slits can easily be made even smaller than the wavelength of light. Jönsson (1961) demonstrated that the region of lateral coherence (§5.6) was up to 60 $\mu$m across the slits.

2.2.4 *Electron mirror interferometer*. The electrons emitted from a source S and accelerated by the potential $V$ of anode $A_1$ are split into two partial beams 1 and 2 by the divergent biprism DB (figure 3); they enter a magnetic prism M of the Castaing and Henry (1964) type, which deflects them by 90° towards an electron mirror. The latter is formed by an anode $A_2$ (held at the same potential $V$ as $A_1$), and by a (bulk) specimen O, kept at a negative potential $V_0(|V_0|>|V|)$. The electrons of the two partial beams are decelerated in the essentially homogeneous mirror field and return at the

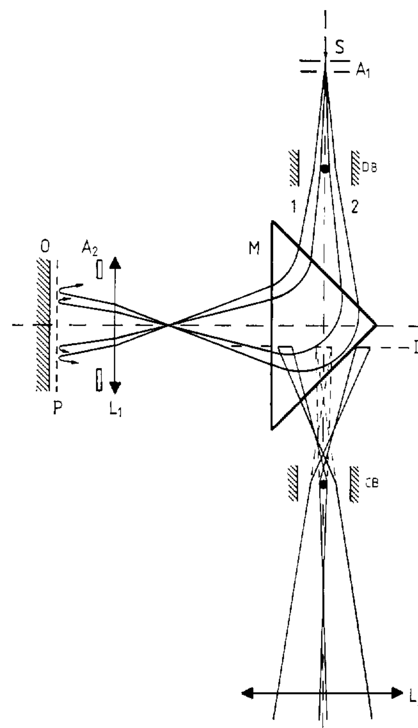


**Figure 3** Schematic set-up of the electron mirror interference microscope. S, electron source; DB, divergent biprism; 1, 2, split beams; M, magnetic prism; $A_1$, gun anode; $A_2$, mirror anode; O, specimen; I, intermediate image plane; CB, convergent biprism; $L_1$, electrostatic lens; $L_2$, intermediate lens.

distance of closest approach (plane **P**) in front of the specimen. While being reflected, the phase of the electron wave is influenced by the local electrostatic field, which in turn is modulated by the topography of the specimen.

The reflected electrons are accelerated by $A_2$ towards M and are bent by another 90° (not indicated in figure 3 for clarity). The setting is such that the focal plane of the electrostatic lens $L_1$ is coincident with the plane of the real stigmatic point of the magnetic prism, and the image plane is coincident with the plane passing through the virtual achromatic and stigmatic point. The combined effect of $L_1$ and M produces a virtual intermediate image (one for each of beams 1 and 2) of the specimen in the intermediate image plane **I**. At the exit from M, the partial beams are deflected towards each other by a convergent biprism CB, so that the two virtual images are superimposed in plane I to form a virtual interference field. A set of lenses $L_2$ placed below CB provides a magnified real image in the viewing plane of the interference pattern, which results from the difference in the phase modulation of the two partial beams 1 and 2 (Lenz 1972).

This electron mirror interferometer has been developed by a German team (Lichte *et al* 1972, Lichte 1977, Lichte and Möllenstedt 1979) with a 25 kV field emission source of 20 nm diameter and a divergence of $2 \times 10^{-4}$ rad (full angle). The two partial beams have a width of about 5 $\mu$m at the specimen and are separated by about 10 $\mu$m.

The device is the analogue of the Michelson interferometer in light optics (Lichte *et al* 1972), with the difference that here parallel (instead of perpendicular) mirrors are used. Details of its applications in the study of surface roughness and microfields are given in §5.5, and of the Doppler effect in §5.7.

The electron mirror interference microscope has also been used (Möllenstedt and Lichte 1978a, 1979) to obtain interference with an arrangement equivalent to the double mirror of Young and Fresnel in light optics. The double-mirror electrode is a conducting echelette grating, held at a potential slightly negative with respect to the cathode, with a lattice constant of 1.6 $\mu$m and groove angles of 5° and 85°. Close to the grating (at about 1 $\mu$m), the reflecting potential varies with the grating periodicity, as do the distance of closest approach and the phase modulation of the reflected electron wave. The incident wave is consequently reflected as if it had impinged on a double mirror with a width equal to the grating spacing, i.e. as if two partial waves were originated by two coherent virtual sources.

2.2.5 *Wavefront and amplitude division interferometer.* A combination of coherent amplitude division produced by a single-crystal film (according to Marton) with wavefront splitting produced by an electron biprism (according to Möllenstedt and Düker) has been used by Matteucci and Pozzi (1980). The diffraction spots formed in the back focal plane of the objective lens when a thin single crystal is irradiated by a parallel beam are used as multiple coherent sources of electrons to illuminate the biprism.

Experiments have been performed in the simplest case of two Bragg spots symmetrically placed with respect to the biprism wire. Four virtual sources are created and a system of lattice fringes is observed in the image plane (conjugate to the specimen plane) with two shadows of the biprism wire superimposed. The crystal has the double function of producing an amplitude splitting of the beam and of being the specimen to be studied.

This arrangement should be suitable for producing off-axis image holograms of specimens placed over the crystal and it might allow the study of crystallographic defects present in the crystal itself. However, further experimental work and a theoretical treatment (lacking at the present) is necessary in order to ascertain if relevant information about the object can actually be obtained.

Kunath (1978) has proposed (see also Hegerl and Hoppe 1970 and §2.1.2) the insertion of the biprism at the level of the condenser aperture in order to obtain two diffraction patterns from a crystalline specimen and to produce interference between two spots of different diffraction order (superimposition is obtained by adjusting the biprism voltage) for the determination of the phase of the structure factors.

## 3 Fundamentals of biprism interferometry

The basic theoretical details related to the physics of the electron biprism and to its application in electron interferometry and interference microscopy will be presented in this section.

### 3.1 *The electron biprism and interferometer*

Since most of the properties of the electron biprism can simply be derived by particle physics considerations, we will follow this approach as far as possible before introducing the wave mechanics treatment.

3.1.1 *Geometrical treatment.* A biprism is formed by a long, conducting wire of radius $r$ charged at a voltage $V_B$ and placed symmetrically between two plates which are kept at ground potential as shown in figure 4, where the axis of the wire is taken in the $y$ direction (normal to the foil) and the electrons are assumed to travel parallel to the $z$ axis.

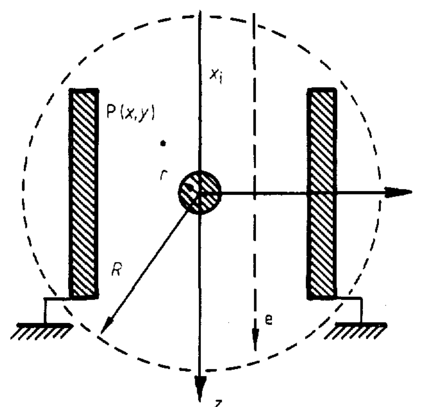


**Figure 4** The electric field distribution near the wire of radius $r$ of a biprism is well approximated by the field of a cylindrical condenser of external radius $R$ and inner radius $r$. $x_i$ is the impact parameter of the electron e.

The properties of the electric field generated by the biprism have been studied by Möllenstedt and Düker (1956) by means of an electrolytic tank in a model one hundred times larger than the actual biprism. The latter was formed by a wire (6 mm long, radius 1 $\mu$m) placed at a distance of 2 mm from the two plates (5 mm long, 2 mm high). It was found that the two-dimensional ($x$, $z$) field distribution so obtained in the region around the wire (where essentially the electron deflections take place) very closely resembles that of a cylindrical condenser with an outer electrode radius $R$ which is of the same order of magnitude as but smaller than the distance between the two plates.

A good approximation of the potential distribution $V(x, y)$ in a point $P(x, z)$ of the biprism is therefore obtained by

assuming that for the screened condenser field (Komrska 1971):

$$V(x, z) = V_B \frac{\ln (x^2+z^2)/R^2}{2 \ln (r/R)} \qquad \text{for } r^2 \leqslant (x^2+z^2) \leqslant R^2$$

$$V(x, z) = 0 \qquad \text{for } R^2 \leqslant (x^2+z^2). \tag{1}$$

An electron of mass $m$ and velocity $v_0$ travelling along $z$ at a distance $x_i$ from the wire suffers an angular deflection $\beta$ given by (weak-field approximation)

$$\beta = \frac{e}{mv_0^2} \int_{-\infty}^{+\infty} \frac{\partial V(x, z)}{\partial x} \mathrm{d}z = \frac{2eV_B}{mv_0^2 \ln (r/R)} \tan^{-1} \frac{(R^2 - x_i^2)^{1/2}}{x_i}. \tag{2}$$

If the wire is positively charged (converging biprism) the electron is deflected towards the wire. In practice, the superposition between the electrons which have been deflected by the wire in opposite direction occurs only for those electrons which travel with an impact parameter $x_i$ of the order of several micrometres. Since the value of $R$ is of a few millimetres, $R \gg x_i$ and equation (2) can be written as

$$\beta = \frac{eV_B \,(\text{sign } x_i)}{mv_0^2 \ln (r/R)} = -\alpha \,(\text{sign } x_i). \tag{3}$$

$\alpha$ is the absolute value of $\beta$, whose sign depends on that of the impact parameter $x_i$. A typical value for $\alpha$ is $10^{-4}$ rad. It is important to note that in this approximation the angular deflection is independent of the impact parameter. The predictions of equation (3) have been confirmed experimentally (Möllenstedt and Düker 1956) up to deflections of $5 \times 10^{-4}$ rad for 44 kV electrons with $V_B = 90$ V and $x_i = 100$ $\mu$m. The latter two values are greater than those used in practice. The independence of $\alpha$ from $x_i$ and the absence of distortion has also been demonstrated theoretically by Septier (1959), who derived an analytical expression for the potential distribution for the case of a biprism with a wire of radius zero placed symmetrically between two earthed planes. Experiments by the same author, performed with 30 kV electrons in an enlarged model where the ratio between the wire diameter and the plate distance was 1:20, have confirmed the validity of the theoretical results up to deflections of $4 \times 10^{-2}$ rad.

As a consequence of the above property, if the biprism is illuminated by a monochromatic electron point source S on the $z$ axis (figure 5), the charged wire will split the electron beam into two partial beams which will appear to originate from two virtual, coherent point sources $S_1$ and $S_2$. They are placed symmetrically with respect to the real source S, and lie in a plane perpendicular to $z$ and containing S at a distance $a$ from the $x$ axis; their separation is

$$d = 2\,|\alpha a|. \tag{4}$$

Typical values for $d$ are 10–50 $\mu$m.

In the region below the wire, where electrons originating from $S_1$ and $S_2$ come together (*overlapping region*, hatched in figure 5), a non-localised interference pattern will be produced. The intersection of the overlapping region with a plane OP (*observation plane*) normal to the $z$ axis at a distance $b$ from the wire and conjugate to the final viewing plane (fluorescent screen of photographic plate) will be called the *interference field*. The width of the interference field $W$ normal to the wire is given by

$$W = 2\left|\frac{a+b}{a}\right| \left(\alpha \frac{ab}{a+b} - r\right). \tag{5}$$

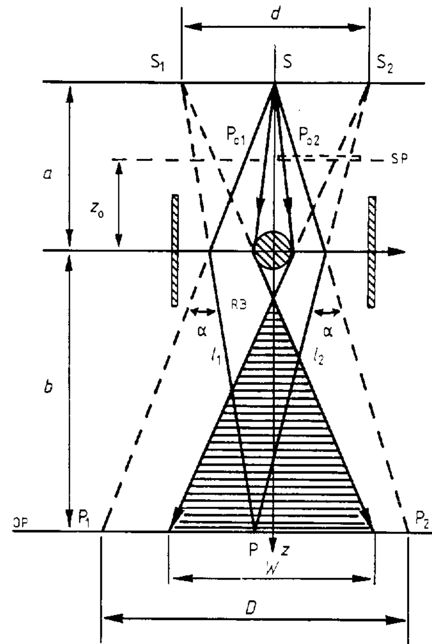


**Figure 5** Basic parameters of an electron biprism illuminated by a monochromatic electron point source S placed on the $z$ axis. $S_1$, $S_2$, virtual sources at distance $d$; $\alpha$, deflection angle; $l_1$, $l_2$, trajectories of two electrons passing through points $P_{01}$, $P_{02}$ in the specimen plane SP and deflected at P in the observation plane OP (instead of passing through $P_1$ and $P_2$) when the biprism is activated; $D$, interference distance; $W$, width of the interference field; RB, reference beam for an off-axis specimen (on the RHS).

It is seen that the interference field will exist ($W > 0$) if

$$\alpha \left(\frac{ab}{a+b}\right) > r. \tag{6}$$

Inequality (6) is an algebraic relation where $a$ and $b$ are conventionally taken to be positive for the case sketched in figure 5 (source S above the wire and observation plane under the wire), and negative in the opposite case, while the sign of the deflection $\alpha$ is the same as that of the applied voltage ($V_B > 0$, convergent biprism; $V_B < 0$, divergent biprism).

The electrons passing through the same given point P (figure 5) of the observation plane OP when the biprism is activated would have arrived at points $P_1$ and $P_2$ in the absence of the biprism; the distance $D$ between these points, termed *interference distance* (see also §3.2), is given by

$$D = 2\,|\alpha b|. \tag{7}$$

Equation (5) shows that $W$ would coincide with $D$ for a wire of infinitely small radius.

In the interference field, a set of straight fringes running parallel to the wire may be observed under suitable conditions to be discussed below (see figure 6). The fringe spacing, $s$, by analogy with the Fresnel biprism, is given by

$$s = \lambda\,|(a+b)/d| \tag{8}$$

where $\lambda$ is the electron wavelength. Since $s$ is of the order of 0.1 $\mu$m, a lens system providing a suitable magnification must be arranged for seeing and recording the fringes on the viewing plane.

The number of fringes $N$ contained in $W$ is given, from

equations (5) and (8), by

$$N = W/s = |(a+b)/ab|(\lambda|b/s| - 2r). \quad (9)$$

For the fringes to be visible, their contrast should be suitably high. By defining the contrast of the fringes as

$$C = (I_{max} - I_{min})/(I_{max} + I_{min}) \quad (10)$$

where $I_{max}$ and $I_{min}$ are the intensities at the maximum and at the minimum respectively (see also §5.6), it can be shown that $C$ is very good, in fact not less than 0.9 (Françon 1956; the different definition of contrast here used is irrelevant to this result) if the transverse source dimension $\delta$ (in the $x$ direction) fulfils the condition

$$\delta \leqslant |as/4b|. \quad (11)$$

This condition states that the angular size of the source must be smaller than the angular size of the fringes when both are seen from the biprism wire. It is equivalent to the well known lateral coherence condition since equation (11) can be written as

$$D \leqslant \tfrac{1}{8}\lambda/\alpha_1$$

where $\alpha_1$ is the semiangle of illumination.

The previous equations have been verified experimentally by several workers and, although diffraction effects are not included, can be usefully applied for the design of the interferometry device and for the setting of the interference microscopes.

The limiting case $W=0$ corresponds to a maximum fringe spacing

$$s_{max} = \lambda|b|/2r \quad (12)$$

and to a minimum virtual source distance

$$d_{min} = 2r|(a+b)/b|. \quad (13)$$

From equations (11) and (12) it turns out that the maximum value allowed for the source size is

$$\delta_{max} < \tfrac{1}{4}\lambda|a|/2r. \quad (14)$$

We wish to draw attention to the important role played by the wire diameter and the source size. In fact, given that $a \simeq 100$ mm and $\lambda = 3.7 \times 10^{-3}$ nm (100 keV electrons) for $r$ ranging from 0.3 to 1 $\mu$m, it turns out that $\delta < 170$ nm and $\delta < 50$ nm respectively.

3.1.2 *Wave treatment.* In the previous section the electrons are considered to be deflected by the field of the biprism; in order to derive the fringe spacing, their wave behaviour has been introduced *ad hoc* by using the analogy with light optics. Diffraction effects have been ignored. We will firstly summarise in this section the wave and quantum mechanics approaches that have been made to describe the propagation of electrons in the biprism. Secondly, we will present an elementary theory of biprism interferometry which, although ignoring diffraction and out-of-focus effects, is adequate for practical purposes.

In the wave treatment, the simplest and very successful model used to describe the biprism is that proposed by Komrska *et al* (1967), which considers the wavefunction in the observation plane OP as the sum of two waves. Each wave describes the diffraction of the electrons originating from a virtual point source by an opaque half-plane. The two half-planes extend in opposite $x$ directions and overlap by the diameter $2r$ of the wire. It can be shown that the above model is exactly equivalent to the description of the biprism according to the following transmission function (Boersch *et al* 1961):

$$\Psi_B(x,y) = \begin{cases} \exp(-2\pi i\alpha|x|/\lambda) & \text{for } |x| \geqslant r \\ 0 & \text{for } |x| < r. \end{cases} \quad (15)$$

Equation (15) holds, within the same limits as equation (3), if the potential distribution around the biprism is given by the cylindrical condenser approximation (equation (1)), whereas it is valid for every value of $x_1$ within the biprism for the model analysed by Septier (1959). A direct derivation of equation (15) can be obtained simply (Matteucci *et al* 1979a) in the phase object approximation (see equation (17)).

By inserting the transmission function (equation (15)) in the Kirchhoff–Fresnel integral, it turns out that the intensity distribution in the observation plane can be expressed in terms of either Fresnel or Hankel functions, depending on whether the illumination is spherical or cylindrical respectively.

A careful comparison between the theoretical predictions and the experimental data has been made by Komrska *et al* (1967). They found a very good agreement between the overall qualitative pattern and the relative intensities of the fringes, which are modulated by diffraction phenomena. In particular, the diffraction fringes present in the shadow of the wire (for $V_B=0$) depend greatly upon the wire diameter which, in turn, can be determined with an accuracy of 2% (Komrska *et al* 1964).

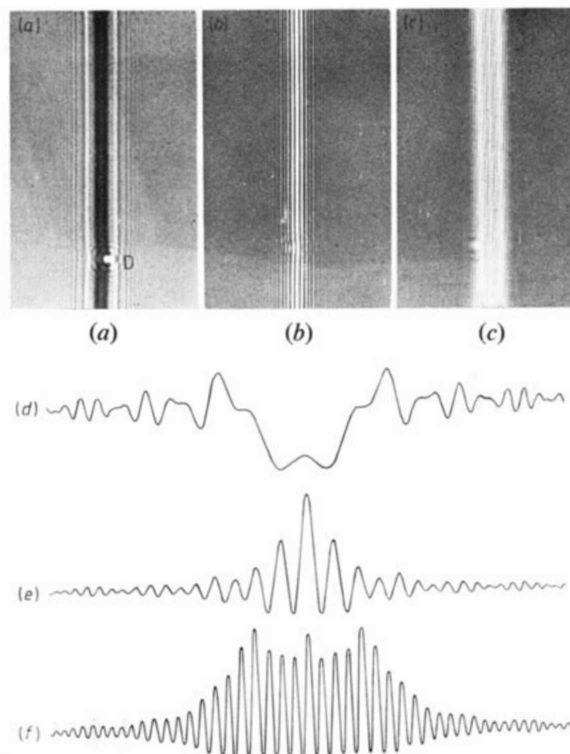


**Figure 6** Electron interference patterns obtained with a convergent biprism without a specimen for wire voltages of 0 (*a*), +4 (*b*) and +8 V (*c*). Parts (*d*), (*e*) and (*f*) show the calculated intensity distributions in the direction perpendicular to the fringes corresponding to (*a*), (*b*) and (*c*), respectively. Note the good agreement. Diffraction effects prevail over interference effects in (*d*), while the situation is reversed in (*e*) and (*f*). Dot D is a bit of dirt on the wire. Accelerating voltage 100 kV; wire diameter 0.49 $\mu$m; $a = 10$ cm; $b = 24$ cm; $\alpha/V_B = 2 \times 10^{-6}$ rad V$^{-1}$.

Anaskin and Stoyanova (1968a, c) have derived the phase of the electron waves scattered by a half-plane from the analysis of the interference patterns and found a good agreement with the calculated values.

A set of experimental fringe patterns and their corresponding calculated profiles is shown in figure 6.

Several efforts have also been made to justify the above model on a conceptually more satisfactory ground. The scattering of electrons by the electrostatic field of the biprism (Komrska and Lenc 1970) has been investigated within the framework of the scalar diffraction theory developed by Komrska (1971) for the case of weak electrostatic fields. The wavefunction in the observation plane can be expressed in terms of the diffraction integral; numerical calculations are, however, necessary in order to derive the intensity distribution of the interference pattern.

The intensities calculated according to the heuristic two-edge model and to the diffraction integral agree, at least within four decimal places; this fact prompted Komrska and Vlachová (1973) to investigate and demonstrate, by means of the method of stationary phase, the equivalence of the two descriptions, which, in turn, justifies the use of the computationally more convenient two-edge model.

Finally, a solution of the Schrödinger and Dirac equations for electrons travelling in the logarithmic potential given by equation (1) around the biprism wire has been worked out by Gesztesy and Pittner (1978a, b, c, d). Although these results are interesting on a theoretical ground, it should, however, be stressed that, from a practical point of view, the two-edge model provides a simple and adequate description for the interpretation of the present experimental data.

We will now suppose that an object is placed in the specimen plane SP (figure 5) at a distance $z_o$ from the biprism plane and is referred to a coordinate system $x_o$, $y_o$ in the SP. (Hereafter the subscript 'o' indicates quantities referred to the object plane.) We remind the reader that in electron interferometry the specimen is always out of focus. The effect of the specimen on the electron beam can be described through a transmission function (object wavefunction) given by

$$\psi(x_o, y_o) = A(x_o, y_o) \exp [i\varphi(x_o, y_o)] \tag{16}$$

where $\varphi(x_o, y_o)$ is the phase term and $A(x_o, y_o)$ represents the amplitude term. In the phase object approximation $A(x_o, y_o) = 1$ and $\varphi(x_o, y_o)$ is given by

$$\varphi(x_o, y_o) = \frac{\pi}{\lambda E} \int_l V(x_o, y_o, z)\, dz - \frac{2\pi e}{h} \int_l A(x_o, y_o, z)\, dz \tag{17}$$

where the integrals are taken along an electron path $l$ parallel to the optical $z$ axis, inside and outside the specimen. $V(x_o, y_o, z)$ is the electrostatic potential and $A(x_o, y_o, z)$ is the magnetic vector potential in the region travelled by the electrons; $e$ is the electron charge, $h$ is Planck's constant and $E$ is a function of the accelerating voltage $V$ given by

$$E = -\frac{V}{2}\frac{2m_0c^2 + eV}{m_0c^2 + eV} \tag{18}$$

where $m_0$ is the electron rest mass and $c$ the vacuum velocity of light.

The main purpose of interferometry is to obtain information on the phase term $\varphi(x_o, y_o)$ through the analysis of the interference pattern.

With reference to figure 5, we will assume that partial beam RB (reference beam) travels in the vacuum while the other split beam traverses the specimen placed off axis. Two rays interfering at the point P, after having passed through two different points $P_{o1}$ and $P_{o2}$ in the specimen plane SP, will have undergone an absolute phase-shift $\Delta\varphi = \varphi(x_{o2}, y_{o2}) - \varphi(x_{o1}, y_{o1})$, since $\varphi(x_{o1}, y_{o1}) = 0$. The fringe pattern which would have been formed in the absence of the specimen will then be modulated by the latter. In the case of a constant phase-shift $\Delta\varphi$, the fringe system is displaced by an amount

$$\Delta s = s\, \Delta\varphi/2\pi. \tag{19}$$

$\Delta\varphi$ is easily obtained by measuring $\Delta s$ and $s$.

In general both partial beams travel through the specimen and therefore $\Delta\varphi$ is a measure of the relative phase-shift between the points $P_{o1}$ and $P_{o2}$.

### 3.2 *Interference electron microscopy*

The purpose of an interference microscope is to produce an in-focus, high-resolution image of a thin specimen and to superimpose on this image the interference pattern produced by the interferometry device, in order to derive additional localised information on the properties of the specimen.

In an interference electron microscope (see figure 11) the final viewing plane VP is therefore conjugate (through lenses) to the observation plane OP and to the specimen plane SP (OP and SP may be coincident) in order to form a focused image of the specimen. It can be seen immediately that it is mandatory for the specimen plane to be always above the biprism plane, in order to obtain a fringe system modulated by the object. In fact, on the contrary, the interfering beams travel through the same object points (see figure 5, assuming SP coincident with OP) and do not, of course, present any phase difference related to the specimen.

Given that the above condition is fulfilled, there are two ways to run the microscope. (*a*) Without any lens between the specimen and the biprism. In this case the observation plane must be coincident with the specimen plane and the biprism must be divergent. (*b*) With one or more lenses between the specimen and the biprism. In this case OP is conjugate to the specimen plane and the biprism will be divergent or convergent according to whether OP is chosen above or below the wire. If OP is coincident with the biprism plane, an in-focus image of the wire (superimposed on the specimen image) is obtained irrespective of the voltage applied to it and no fringe system is visible.

When $V_B = 0$ and the specimen is removed, a shadow image of the biprism wire (together with diffraction effects) is formed on the viewing plane irrespective of the operating condition (*a*) or (*b*) adopted. By inserting the specimen, its in-focus image is obtained, although it is partly hidden by the shadow of the wire.

The portions of the image on the left and on the right of the shadow are of the same extension, provided that the wire is centred on the optical axis.

The specimen image wavefunction in the presence of the biprism can be calculated, according to Glaser's paraxial theory (Glaser 1952, 1956), by following the propagation of the wavefunction through the microscope in two steps, the first step being from the object (equation (16)) to the biprism and the second step being from the biprism, which is described by the transmission function (15), to the image.

The resulting wavefunction is complicated but the main features of the image, including diffraction effects (which are important when the width of the interference field is of the same order of magnitude as the Fresnel fringe width of the biprism), can be derived using the asymptotic approximation (Pozzi 1975, 1980) assuming that the electron wavelength is the small parameter.

The shadow of the wire may be distorted if the first partial derivative of the phase $\varphi(x_o, y_o)$ (equation (17)) in the direction

normal to the wire axis is different from zero (Schlieren effect, see figure 10(*a*), §5.4); similarly, the second derivative affects the spacing of the diffraction fringes at the edge of the shadow of the wire. These effects are independent of the voltage applied to the wire and may be used to detect local electric and magnetic fields and thickness variation in the specimen.

On applying a bias voltage to the biprism, the distorted shadow will widen or shrink depending on the overall electron optical conditions. In the case of shrinkage, by increasing $V_B$, the LHS and RHS partial images (corresponding to two different regions of the specimen) move towards each other in a direction perpendicular to the wire by an amount $\pm\frac{1}{2}D_o$ proportional to $V_B$ (see equations (3) and (7)) until the shadow disappears. When the voltage is increased further, the two images overlap and an interference field is produced (equation (5)). It should be noted that the boundaries of the interference field, together with diffraction effects, have the same profile as that of the distorted shadow (see figure 10(*b*)), although with left–right inversion.

When the interference field is much larger than the first Fresnel fringe width, the diffraction effects due to the wire edges do not affect the trend of the interference fringes appreciably in the central part of the interference field and can be neglected. These favourable conditions are encountered where a highly coherent source is used (typically a field emission source).

Assuming an ideal imaging system, the wavefunction in the specimen plane and within the interference field can then be described by

$$\psi = \psi[(x_o - \tfrac{1}{2} D_o), y_o] \exp(i\pi x_o/s_o) + \psi[(x_o + \tfrac{1}{2} D_o), y_o] \exp(-i\pi x_o/s_o). \quad (20)$$

In the absence of an object, an interference fringe system is present in the viewing plane; the corresponding spacing, referred to the specimen plane, is $s_o$.

The trend of this fringe system is modified by the phase term $\varphi$ which is introduced by the object; information can then be obtained about the phase term itself. More precisely, information on the phase difference between points distance $D_o$ apart is again obtained from the fringe system. If, however, an interesting region of the object overlaps a structureless region ($A=1$, $\varphi=0$, e.g. a hole) then information on the absolute phase can be obtained. In this respect the interference distance $D_o$ is an important parameter; it depends on the observation conditions (see equation (7)) which can be varied within a wide range.

For a given setting, $D_o$ may be derived easily once the biprism has been calibrated in terms of image displacement per unit voltage applied to the wire and once the total magnification $M_T$ of the microscope is known. The calibration is performed by measuring, in the final screen, the change in distance $\Delta D'$ between two image points situated on a line perpendicular to the wire axis and on opposite sides of it for a given change in the wire voltage $\Delta V_B$. The value of $D_o$ for a voltage $V_B$ is then given by

$$D_o = (\Delta D'/\Delta V_B)\, V_B M_T^{-1}. \quad (21)$$

$D_o$ ranges from 5 to 500 nm $V^{-1}$.

When OP is not coincident with SP, the proper magnification factor must be used in equation (21) in order to obtain $D$. A similar procedure may be used for deriving $s_o$, $W_o$ and $s$, $W$.

No loss of resolution of the object wavefunction is predicted by the analysis of the first two terms of the expansion obtained with the asymptotic approximation. This has been taken for granted by nearly all workers. However, the analysis of the spatial frequencies transmitted by the biprism made by Wahl (1975) in connection with electron holography has shown that not all the spatial frequencies are equally transmitted to the image and that the filtering effect is greater for points closer to the edges of the interference field. This effect has not yet been treated theoretically from the wave optics point of view; it could be responsible for the presence of ghost images of the specimen, for which a simple geometrical explanation has been given by Faget (1961).

## 4 Instrumentation

A general description of the features of electron interferometers and of interference electron microscopes will be given. The description is preceeded by practical considerations of the biprism assembly, which is a common part of both instruments.

### 4.1 *Practical considerations about the biprism*

The key item is the wire, which should be very thin (less than 1 $\mu$m in diameter), straight, clean, robust, electrically conductive and a few millimetres long. Materials used comprise quartz and borosilicate glass (0.2 to 2 $\mu$m diameter), from which wires are produced by pulling a rod over a Bunsen flame, and spider's web (0.1 to 0.4 $\mu$m diameter), fabricated by very small spiders, which has the advantage of presenting some elasticity. All these wires, because they are made from insulators, require a metal coating, which is obtained by subsequent vacuum evaporation of chrome and gold; quartz and borosilicate glass wires are brittle and the coating may easily lose its electrical conductivity. Metal wires are more satisfactory: tungsten wires can be thinned down electrolytically to 1 $\mu$m (Tomita *et al* 1972) while platinum wires, stripped chemically from Wollaston wire, can have a diameter as low as 0.3 $\mu$m (Matteucci 1978).

A selected portion of wire is glued at its ends using conductive adhesive on to two electrically insulated pads which are mounted in a frame carrying the earthed plates of the biprism. Care is taken to place the wire symmetrically with respect to the plates. Failure to do so affects the central fringe of the interference pattern, which is no longer of low order. Provisions for applying a voltage to the wire are also made.

The mounting of the wire requires a great deal of skill because of its small size and the constraints imposed by its shape. The quality of the wire is checked directly in an electron microscope by examining its shadow. After a period of use (of several hours) a contamination layer builds up around the wire; this adversely affects the image quality but treatment of the whole biprism for a few minutes in a RF sputtering apparatus usually restores its performance (Vittori-Antisari and Valdrè 1977).

Details of the wire production and mounting can be found in the literature (see e.g., Faget 1961, Fert *et al* 1962, Hibi and Yada 1976).

### 4.2 *Electron interferometers*

An electron interferometer comprises the electron source, the condenser system, the specimen air lock, the interferometry device, the magnification lenses and the recording system (figure 2).

Electron interferometers produce only an interferogram of the specimen; no image is made. They are usually electron optical benches set up for the purpose, and can be equipped either with electrostatic lenses or with magnetic lenses. Only one interferometer, built for trial, uses a combination of both type of lens (Hibi and Takahashi 1963).

If the electron gun is based on a conventional thermoemitter, (hairpin filament), the necessity of conveying sufficient electron current to the interferogram makes mandatory the

use of a line source (rather than a round one), which should be parallel to the biprism wire. This source may be formed by a slit-type aperture (a few microns in width) and cylindrical electrostatic lenses (Düker 1955, Möllenstedt and Düker 1956) (for both illumination and the magnification system), which present minimum alignment problems between the slit and the wire. On the other hand, electrostatic lenses can be used only with low accelerating voltages (up to 60 kV), which adversely affects the gun brightness, the specimen penetration and, for a given specimen thickness, the coherence of the beam.

These disadvantages are not shared by magnetic lenses (for which the accelerating voltage usually ranges up to 100 kV), and the problem of image rotation introduced by them, which changes on varying their excitation, can be overcome by suitable lens excitations and by providing mechanical adjustments for the biprism and for the slit aperture (Faget and Fert 1957b). Alternatively, an additional rotation lens can be introduced into the electron optical bench (Faget 1961).

Magnetic quadrupoles, originally proposed for the magnification system (Faget and Fert 1957b), are an interesting proposition: their convergent–divergent properties along two orthogonal directions provide (i) an increased fringe spacing, (ii) a reduction of magnification along the biprism axis, thus increasing the electron density in the interferogram (see, for instance, figure 7), and (iii) a ready made linear source when used as a condenser.

Electron interferometers equipped with magnetic quadrupoles have been built for work at high voltages (Kerschbaumer 1967 (for 100 kV electrons), Schaal 1971, Schiebel 1979 (up to 300 kV electrons)).

On the other hand, the use of relatively low voltages (between 2 and 5 kV) may present several advantages with respect to mechanical and alignment problems and to the shielding from spurious magnetic fields (Hasselbach 1979). In this respect systems of compensating coils have been developed (Buhl 1961b) which can reduce spurious alternating fields down to $6\times10^{-8}$ A m$^{-1}$. Interference by means of 150 V electrons, decelerated by a retarding electrostatic lens, has been obtained from a biprism wire as large as 10 $\mu$m in diameter by Fischer and Lischke (1967).

The small cathode size of the pointed filaments and their higher coherence with respect to hairpin filaments dispense with the need for cylindrical and quadrupole lenses (Hibi and Takahashi 1963, Sonier 1968).

The adoption of field emission guns represents, however, the best solution: their extremely high brightness and coherence make even the condenser system redundant (Brünger 1968, Crewe and Saxon 1970, Hasselbach 1979).

The specimen can be inserted into the electron interferometer, via an air lock, at various levels; in any case it has to intercept only one of the interfering electron beams.

The interferometry device is located below the final condenser and it should be easily removed from the machine for inspection and cleaning.

Recording is usually performed with high-speed photographic emulsions. An image intensifier has proved to be very useful for this work in order to set the right experimental conditions before photographic recording, and also for following time-dependent effects (Söllig 1974, Lichte 1977, Hasselbach 1979).

### 4.3 *Interference electron microscopes*

These represent the natural extension of the electron interferometer, where one or more further lens is added to provide an image of the specimen overlapped with the interference pattern.

Interference microscopes were developed as soon as experimental evidence was available on the preservation of the coherence of the electron waves which had travelled through thin specimens. Gabor (1956) arrived at the same conclusion on a theoretical ground.

A common feature of early types of interference microscope is the adoption of a slit source for intensity reasons and of a biprism as an interferometry device. Two distinct versions are that of Möllenstedt and Buhl (1957) and Buhl (1958, 1959) and that of Faget and Fert (1957b) and Fert *et al* (1962). The interference microscope of Möllenstedt and Buhl comprises (i) an electron microscope with electrostatic lenses, (ii) a double cylindrical condenser lens and (iii) a biprism which is located between the specimen and the objective lens. On the other hand, the Fert and Faget type comprises (i) an electron microscope with magnetic lenses, (ii) a double condenser lens with a slit aperture and (iii) a biprism which is located under the objective lens. A similar set-up has been used by Drahoš and Delong (1963) and Anaskin *et al* (1966) in commercial microscopes. The first arrangement produces highly magnified fringes and the second a highly magnified image.

The French workers used two subsidiary sets of apparatus to obtain satisfactory interference fringes. Specifically, a rotation magnetic lens was placed under the condenser lens so that the image of the condenser slit aperture could be rotated in order to be correctly superimposed on the wire of the biprism. In addition, a quadrupole magnetic lens was inserted after the projection lens; by adjusting the excitation current of the quadrupole lens, an interference fringe system of very high contrast could be clearly seen.

The biprisms have been implemented with facilities for traverse, rotation (for orientation along preferential directions; in particular, in the case of linear sources, along their axes) and translation along the microscope axis.

The introduction of pointed filaments marked a great progress, since they made the slit source and the cylindrical lenses redundant, as first demonstrated by Feltynowski (1963) and Hibi and Takahashi (1963). Feltynowski used an Elmiskop 1 with the biprism inserted at the level of the diffraction aperture plane while the instrument developed by Hibi and Takahashi was based on (i) an electrostatic microscope, (ii) a double condenser system and (iii) a biprism located under the objective lens. Sonier (1971) assembled an interference microscope by using standard components of conventional magnetic electron microscopes and a biprism. Finally, several commercial types of electron microscope were used as interference microscopes, simply by mounting pointed filaments and by the incorporation of a biprism, which is usually placed at the level of the diffraction aperture (Feltynowski 1963, Unwin 1971, Yada *et al* 1973, Merli *et al* 1974a) or above it (Tomita *et al* 1972).

Nowadays, practically every type of microscope can be used for electron interferometry without affecting its performance, in fact rather increasing its potentials. Specimen magnifications up to $10^5\times$ are possible in instruments equipped with three lenses after the specimen, if the biprism is placed at the level of the diffraction aperture. An interference kit is even available from one maker (Tesla) of electron microscopes. To ease the use of a microscope for interferometry and to gain in flexibility, the instrument should incorporate facilities for free-lens operation, not always available in modern, preprogrammed microscopes.

The high-magnification interferograms can hardly be seen on a fluorescent screen, unless a field emission gun is used (Munch 1975, Tonomura *et al* 1978), even after long periods of adaptation of the dark; they are usually taken blindly. Fringes may be recorded on high-speed photographic plates with exposure times as high as 200 s. An image intensifier is a

useful ancillary device for adjustment purposes (see Wahl 1973).

## 5 Applications

Electron interferometry and interference electron microscopy have been applied in several distinct fields to measure quantities such as inner and contact potentials, specimen thickness, trapped magnetic flux and electron source coherence, to study magnetic domains and p–n junction electric fields, and to provide holograms for off-axis electron holography. In this section a concise review of the above applications will be given.

### 5.1 *Measurement of mean inner potentials and specimen thickness*

The measurement of the refractive properties of thin films was the earliest and has so far been the most extensive application of electron interferometry. The mean inner potential $V_m$ is the first term of the Fourier expansion of the potential in a crystal and it is of the order of 10 V. If a material of thickness $t$ is traversed by one split beam of the interferometer (the other split beam travelling in a vacuum) a phase difference (see equation 17))

$$\Delta\varphi=(\pi/\lambda E)\,V_m t \tag{22}$$

is produced between the two beams, where $E$ is defined by equation (18). A shift $\Delta s$ will occur in the fringe system of spacing $s$, produced by the interferometer in correspondence with the specimen, such that (see equation (19))

$$\frac{\Delta s}{s}=\frac{\Delta\varphi}{2\pi}=\frac{V_m\cdot t}{V\cdot\lambda}\cdot\frac{m_0c^2+eV}{2m_0c^2+eV} \tag{23}$$

where $V$ is the voltage applied to the gun. $V_m$ can then be calculated from the measurements of $s$, $\Delta s$ and the thickness $t$. $t$ is usually measured using optical methods. Alternatively, if $V_m$ is known, equation (23) can provide a means for thickness measurements. In order to measure $\Delta s$, the specimen should be smaller than the extent of the fringe system, which means that it should be in the form of an island or needles, or it should have free edges. An example of fringe shift taking place in these type of measurements is presented in figure 7.

The precision of the method can be of the order of a few

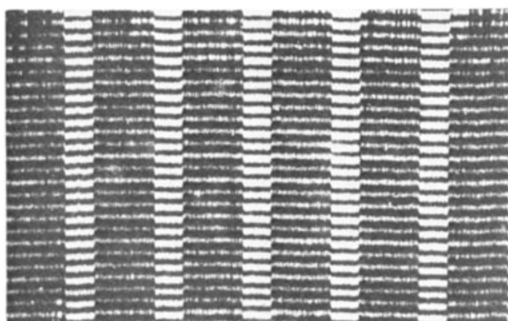

Figure 7 Fringe pattern, in measurements of mean inner potentials $V_m$, produced by interference between one electron beam passing through an Al reference region (substrate) of constant thickness and one beam passing through a known thickness $t$ (10 nm) of Al deposited, grating-like with a periodicity of 50 $\mu$m, on top of the substrate. The shift of the fringes is proportional to $V_m t$. The wider stripes correspond to the thicker regions of the specimen. The accelerating voltage was 60 kV. The magnification in the direction of the fringes is higher than in the orthogonal direction because cylindrical lenses have been used.

per cent, which is slightly worse than that of electron diffraction measurements (Hibi and Yada 1976), but it has the advantage of being related to very localised regions of the specimen.

Some precautions must be taken in these measurements. For instance, to prevent the effect of contact potentials, the same material is used for the specimen and its support (figure 7), or the specimen is made self-supporting (Möllenstedt and Keller 1957, Langbein 1958, Keller 1958, 1961a, Hoffmann and Jönsson 1965, Jönsson *et al* 1965); in order to guarantee the planarity of the specimen, recourse is made to surface tension in the preparation of the films; to reduce the presence of contaminants, controlled preparation and environment conditions are used.

Improvements in the precision of the measurements can be obtained by working with thick specimens, that is, with high accelerating voltages (Kerschbaumer 1967). Gold of thickness up to 40 nm has been used with a gun voltage of 300 kV (Schaal 1971).

In the field of interference electron microscopy an accurate study has been performed by Yada *et al* (1973) and Hibi and Yada (1976) of the factors which may affect the measurements of the mean inner potential: for instance, specimen position with respect to the fringe system, specimen orientation with respect to the beam, in particular at the Bragg reflecting position, and focusing of the image. They found that the specimen edge should be located in the vicinity of the central fringe of the interferogram, that the mean inner potential varies critically (even by a factor 2.5) for specimen orientations very close to the Bragg reflecting positions (the true $V_m$ is that derived at the off-Bragg positions) and that the specimen should be at the exact focus or slightly over focus. The latter effect has been interpreted as being due to the refraction of the electrons when entering and leaving a non-plane specimen (Berger *et al* 1980).

For details on the great variety of specimen preparation, see Faget and Fert (1957a, b), Durand *et al* (1958), Buhl (1958, 1959), Anaskin and Stoyanova (1968b), Tomita and Savelli (1968), Sonier (1970, 1971) and Berger *et al* (1980).

### 5.2 *Measurement of contact potentials*

The measurement of contact potentials between two materials A and B can be performed by coating the wire of the biprism with an evaporated layer of A, which is subsequently partly covered along its length with a layer of B (Krimmel *et al* 1964). The effective potential in the B part of the wire is the sum of the applied voltage $V_0$ and the contact potential between the materials A and B. The interferogram will then show two different sets of fringe spacings from which the contact potential can be derived. Early experiments showed that a surface layer of residual gases caused variation of the contact potential. An electron interferometer operating at about $10^{-7}$ Pa ($10^{-9}$ Torr) and equipped with a field emission source has been built (Brünger 1968). The material under investigation is evaporated *in situ* and the contact potential is recorded dynamically in the following way (Brünger 1971, 1972, Brünger and Klein 1977). The fringe system produced by A is observed on a fluorescent screen where it is superimposed on a mask formed by a linear grating; in general a moiré pattern will be visible. The wire voltage is then adjusted up to the value $V_0$ at which the moiré pattern disappears, which means that the fringe spacing is equal to that of the grating. In some experiments (e.g. evaporation of material B, or gas inlet at a given pressure), the wire voltage is kept adjusted for absence of moiré pattern. The voltage change $\Delta V$ is therefore a direct measurement of the contact potential, which can be studied dynamically in this way. The accuracy of this method

is of a few per cent and is comparable with that obtained with the vibrating capacitor method (Huber 1966).

5.3 *Measurement of trapped magnetic flux*

Under this heading the detection and measurement of magnetic flux changes are considered. The great sensitivity of electron interferometry to small flux changes has produced the first direct evidence of the connection between the vector potential and the electron optics refractive index (as originally pointed out by Ehrenberg and Siday (1949)), and the first direct measurement of the quantum of flux.

If the trajectories $l_1$ and $l_2$ of the two interfering electron beams originated by source S (figure 5) comprise a region where the vector potential $A(x, y, z)$ is not zero (although the flux density $\boldsymbol{B}$ may be zero along $l_1$, $l_2$), a phase-shift $\Delta\varphi$ is produced, given by (see equation (17), §3.2.1)

$$\Delta\varphi=\frac{2\pi e}{h}\left(\int_{l_1} A(x,y,z)\,\mathrm{d}l-\int_{l_2} A(x,y,z)\,\mathrm{d}l\right)=\frac{2\pi e}{h}\varphi(\boldsymbol{B}) \quad (24)$$

where $\varphi(\boldsymbol{B})$ is the flux linked with $l_1+l_2$. A phase-shift of $2\pi$ is produced by a flux

$$\varphi(\boldsymbol{B})=2\Phi_0=h/e=4.13\times10^{-15}\ \mathrm{T}$$

$(=4.13\times10^{-7}\ \mathrm{G\ cm^2})$.

Several experiments of electron interferometry have been performed (Chambers 1960, Fowler *et al* 1961, Boersch *et al* 1961, 1962a) in order to show that the vector potential, rather than the flux density, is responsible for phase-shifts (Aharonov–Bohm paradox); however, the experimental set-up which most closely complies with the spirit of the paradox is that carried out by Möllenstedt and Bayh (1962) and Bayh (1962). An interferometry device made up of three cascade biprisms is used (see §2.2.1.1) in order to get a wide separation, up to 60 $\mu$m, in which to place a small solenoid (Möllenstedt and Krimmel 1963). The magnetic flux $\Phi(\boldsymbol{B})$ produced by the solenoid is given by $\pi r^2 B$, where $r$ is the external radius of the coil ($<10\ \mu$m) and $\boldsymbol{B}$ is the flux density. $\boldsymbol{B}$ is proportional to the current flowing in the coil and can be considered to be different from zero only inside the long solenoid. The current is varied while the interference pattern is recorded on a photographic film (which slides in the direction of the axis of the biprism wire) through a slit normal to the axis of the wire. The results are clearly shown in figure 8, where the spacing of the interference fringes is much smaller than that of the Fresnel diffraction fringes (cf figure 6 where this is not the case, owing to different electron optical conditions). The interference fringes (extending all over the picture) shift continuously on varying the coil current, while the shape of the central interference field and of the diffraction fringes at both sides of it remains straight, confirming that the Lorentz force acting on the electrons is negligible. The best results show that the current required to produce a shift of $2\pi$ is such that $\varphi=4.15\times10^{-15}$ T, with a precision of 1.5% (Schaal *et al* 1966/7). In addition, it has been shown that the magnetic flux produced by currents flowing in normal conductors is not quantised.

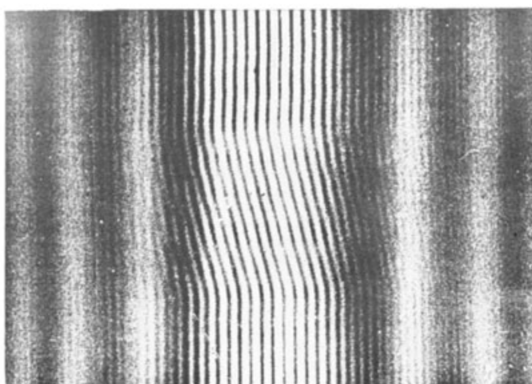

**Figure 8** Dynamically recorded fringe system showing the displacement caused by a continuously varying magnetic flux produced by means of a microcoil inserted between the split beams of the biprism.

Magnetic flux quantisation may occur, on the other hand, in superconductors. Detection and measurements of flux quanta (fluxons) have been performed by electron interferometry. A small hollow cylinder of superconductor is placed between the two beams of an interferometer (Wahl 1968/9, 1970a, b) or a superconductor is evaporated over the biprism wire (Lischke 1969). The superconductor is cooled below its transition temperature in a magnetic field. As the external field is removed, a quantised magnetic flux is trapped in the hollow superconductor. Thermally activated flux changes can be followed on the interferograms. The following results have been obtained (Boersch and Lischke 1970a, b, Lischke 1970a, b).

(1) For thick-walled cylinders (0.2 $\mu$m) the interferograms showed only changes of one half spacing (i.e. a bright fringe interchanged with a dark one following the escape of one fluxon (figure 9)), or by multiples of it, that is, the flux was found to be quantised in units $\Phi_0=h/2e=2.07\times10^{-15}$ T, in agreement with the theory, within an accuracy of 20% for a single fluxon. By measuring the effect produced by seven fluxons, the experimental error was 4%.

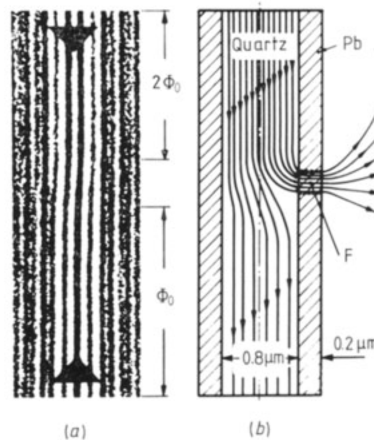


**Figure 9** (*a*) Interferogram showing the variation of an interference fringe system as a consequence of the escape of one fluxon from a magnetic flux trapped in a superconducting lead cylinder. (*b*) Schematic representation of the arrangement, showing flux creeping at F. (Courtesy of *Physica Status Solidi.*)

(2) No differences between the flux changes and the quantum unit $\Phi_0=h/2e$ were found near the transition temperature, contrary to the theoretical predictions.

(3) The flux distribution along a cylinder was found not to be constant and fluxons down to 8 $\mu$m in length were observed. The method is sensitive enough to investigate flux creep. A steady flux speed of 1 nm s$^{-1}$ can be detected at a single flux quantum $\Phi_0$.

These results have led to a permanent set-up, called a vortex microscope, for the study of single flux lines, capable of a resolution of 0.5 $\mu$m (Boersch *et al* 1974a, Söllig 1974). It

is possible to detect flux jumps between pinning centres and, in conjunction with surface decoration techniques, to study the interaction between single flux lines and specific pinning centres (Boersch *et al* 1974b, Söllig 1974, Rodewald 1977).

Although this method has an accuracy not comparable to the extremely high accuracy of the SQUID method, it has the great advantage of a spatial resolution 100 times better (Söllig 1974).

### 5.4 *Studies of electric and magnetic fields*

These studies are usually performed using out-of-focus techniques or the displaced aperture method (for a recent review see Jakubovics 1976); almost all the work has been concentrated on magnetic materials and only a few attempts have been devoted to the observation of p–n junctions in silicon by out-of-focus TEM (Merli *et al* 1975) and STEM (Darlington and Valdrè 1975).

Interference electron microscopy provides a new in-focus technique for the above studies (Matteucci *et al* 1979b).

It had been hoped that it would be possible to get a better understanding of the structure of magnetic domain walls by this method. So far all that have been obtained are measurements of the phase change occurring in 180° domains (Tonomura 1972), the determination of whether the domain walls are convergent or divergent (Pozzi and Missiroli 1973), estimates of the domain wall width (Martelli *et al* 1978) and mapping of magnetic field distribution (Wahl and Lau 1979, Tonomura *et al* 1980).

The interferograms are in qualitative agreement with the theory, which predicts a fringe shift at the domain walls and a deformation of the boundary of the interference field (§3.2) independent of the biprism voltage (figure 10).

In the case of p–n junctions, interferometry has been used to locate the depletion region; however, the aim of establishing correlations with crystallographic defects present in the material and imaged by diffraction contrast has been hampered by the low magnification available (Merli *et al* 1974b, 1976b). Detectable phase-shifts may be obtained only if the depletion region is narrow (a few tens of nm) or, for wide junctions (several $\mu$m), if the interfering beams have travelled on either side of the junction.

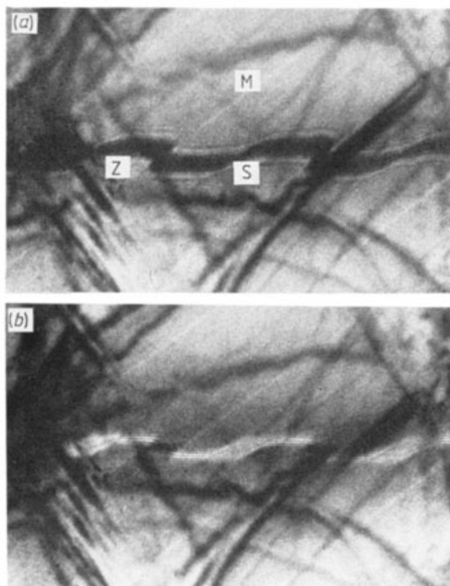


**Figure 10** Image of a thin cobalt specimen with the shadow of the biprism wire superimposed: (*a*) $V_B = 0$ V, with diffraction fringes; (*b*) $V_B = +9$ V, with interference and diffraction patterns. Because the images are slightly out of focus, the magnetic domain walls M are visible by Fresnel contrast. Note the zig-zag (Z) and step (S) effects at the intersections of the domain walls with the shadow of the wire. Width of field of view, 1 $\mu$m.

Other applications concern the measurements of the potential acquired by a non-conducting wire as a consequence of charging up by electron irradiation (Unwin 1971). The potential was deduced from an analysis of the interference fringe system. The wire was then used as a phase-shifting device.

Recently, the electric field distribution in the proximity of the tip of a field emission cathode held at various voltages has been investigated by using the tip as the specimen in an interference electron microscope (Kulyupin *et al* 1978/9).

### 5.5 *Surface studies*

The electron mirror interferometer (§2.2.4) has been used for the assessment of surface smoothness and for the measurement of the roughness of highly polished surfaces of glass used as x-ray reflectors (Lichte and Möllenstedt 1977, 1979, Lichte 1977, 1979). The mirror specimen is coated with a thin layer (20 nm) of gold in a vapour blast process to assure electrical conductivity. If its surface is not completely flat, the electrostatic field in front of it deviates from uniformity and the phases of both the partial waves produced by the first biprism are changed by different amounts; this effect is stronger the closer the electrons approach the mirror surface. On decreasing the negative voltage applied to the mirror, the uneveness of its surface shows up as an increased fringe shift in the interferogram produced by the second biprism.

The resolving power for variation of specimen height depends on the surface structure. In the case of a sinusoidal variation of height with a lateral periodicity of 1 $\mu$m, the resolution is 0.2 nm and improves to 40 pm for a spacing of 5 $\mu$m.

The results obtained agree within experimental error with the values derived for the same specimen by using x-ray scattering. The sensitivity of the two methods is comparable.

### 5.6 *Measurement of coherence and brightness*

Since interference can take place only between coherent waves, it can provide a means for measuring the degree of coherence of an electron source and the effect of a specimen on the coherence of a wave (for a general review see Hawkes 1978).

We will deal here only with the space coherence (coherence length) of a source and with the specimen interaction, since Gabor (1956) has shown that the time coherence is always fulfilled (electron wavepackets have a length of the order of $5 \times 10^5$ wavelengths against the path differences of $10^3$–$10^4$ wavelengths usually involved in interference experiments with electrons).

Simpson (1954) gives a theoretical estimate of 5600 wavelengths for the mean path difference in the three-crystal interferometer device (§2.1.1). In an interference experiment with an electron biprism, the maximum path difference from one side to the other of the interference field is given by $N\lambda$, $N$ being the number of fringes defined in equation (9). The best results so far obtained give $N > 3000$ for a field emission gun (Tonomura *et al* 1979d) and $N = 2200$ for a linear thermo-ionic source (Keller 1961b).

It is well known from light optics that the visibility of interference fringes depends on the source size. The visibility, or contrast, is a measure of the spatial coherence of the source and, therefore, of the source size. Assume that $I_1$ and $I_2$ are the intensities that sources $S_1$ and $S_2$ (figure 5) will separately

produce at a point on the observation plane. Where the waves interfere, the resulting intensity will be (ignoring diffraction effects)

$$I=I_1+I_2+2(I_1I_2)^{1/2}|\gamma_{12}|\cos\chi. \quad (25)$$

$\chi$ is a linear function of the path difference only, and $\gamma_{12}$ is the normalised degree of coherence of the waves. For the biprism $I_1=I_2$ and the two waves are synchronous (i.e. $\gamma_{12}$ is a real number); if the contrast is defined according to equation (10), it turns out that

$$C=|\gamma_{12}|.$$

For a slit source of width $\delta$ (and approximately for a circular source of diameter $\delta$), $|\gamma_{12}|$ is given by (Sonier 1971)

$$|\gamma_{12}|=\frac{\sin(\pi\delta/\sigma)}{\pi\delta/\sigma} \quad (26)$$

where

$$\sigma=|sa/b|=|\lambda(a+b)/2\alpha b|. \quad (27)$$

The fringes disappear ($\gamma_{12}=0$) for $\delta=n\sigma$ ($n$ being an integer), while their contrast is maximum ($\gamma_{12}=1$) for $\delta\ll\sigma$. Periodic reversals of contrast take place on decreasing $\sigma$, the central fringe going from bright to dark, while the visibility decreases. Experiments confirm these predictions (Faget *et al* 1958, Faget 1961, Drahoš and Delong 1964, Sonier 1971).

From a densitometer trace of an interferogram, equation (26) allows the measurement of the degree of spatial coherence. In this way the effect of the various parameters entering in equation (26), such as the size of the electron source and the diameter of the wire (for which agreement was found within errors of 4% and 3% respectively), the wire potential and the source-to-wire distance, has been investigated (Hibi and Takahashi 1969). In addition, the effect of the bias resistance of the electron gun and of the temperature of the (point) cathode have been considered. In particular, an increase of $\gamma_{12}$ with temperature, which implies a decrease of the effective source size, was found.

Anaskin and Stoyanova (1968f) have derived expressions for the contrast $|\gamma_{12}|$ in the cases of non-monochromatic sources, of sources of finite width and different intensity distributions, and of mechanical instabilities. The predictions are satisfactorily verified experimentally.

The normalised intensity distribution of an electron source can be obtained from the contrast measured in interferograms taken at different biprism voltages, according to the Cittert–Zernike theorem (see Hawkes 1978). Braun (1972) has compared the theoretical distribution calculated according to this method with the experimental one obtained by measuring the electron current distribution in the image of the source (a pointed filament) and found good agreement.

In other works (Burge *et al* 1975, 1976) the performances of various types of electron cathodes have been compared, and an increase in the coherence by a factor of two was found in going from a conventional hairpin cathode to a thermo-ionic point filament.

Speidel and Kurz (1977) and Kurz (1979) have investigated the dependence of the source size of a field emission gun on the magnetic stray fields of their laboratory. By measuring the electron current using a Faraday cup, they were able to determine the axial brightness of the source. Similarly, Möllenstedt *et al* (1978) have estimated the brightness of a laser-heated electron gun.

The measurements of spatial coherence by electron interferometry have an accuracy of about 4–5%, which is slightly better than that obtained by the analysis of Young's fringes produced by superimposing two micrographs of an amorphous specimen in an optical diffractometer (Frank 1976, Frank *et al* 1978/9). Other methods (see Hawkes 1978) have been used only qualitatively.

Simulation of chromatic effects (such as in light optics) have been performed by applying an alternating voltage to the wire; this produces a superimposition of fringes with different periodicities on the photographic plate (Möllenstedt and Düker 1956, Faget *et al* 1958).

The measured decrease in $\gamma_{12}$ when an object is interposed in the ray path (carbon (Menu and Evrard 1971, Hibi 1974, Burge *et al* 1975), collodion and germanium (Hibi 1974) and biological specimens (Hibi and Takahashi 1969, 1971, Hibi 1974, Hibi and Yada 1976)) confirms that inelastically diffused electrons contribute to the background, i.e. the interferometer acts as a filter between the electrons which are elastically scattered (coherently scattered) and those which are inelastically scattered (incoherently scattered). Electron micrographs of non-biological and various types of biological specimens have been taken for different values of $\gamma_{12}$ (up to 0.6). The contrast is consistently higher, up to a factor three, for those images which were taken with a higher value of $\gamma_{12}$ (Hibi and Yada 1976).

### 5.7 *Basic and teaching experiments*

The complete similarity between the de Broglie electron wavelength and the wavelength of electromagnetic radiation has been confirmed, by using both electrical and magnetic fields, in a large number of experiments whose counterparts in light optics are (i) the Fresnel biprism (§2.2.1), (ii) the Young interferometer with holes and slits (§2.2.3), (iii) the Young–Fresnel double mirror (§2.2.4) and (iv) the Michelson interferometer (§2.2.4). In addition, the equivalent of the Mach–Zehnder interferometer has been realised (§2.1.1).

Recent experiments have also demonstrated successfully the occurrence of Doppler shift in the electron waves (Lichte 1977, Möllenstedt and Lichte 1978b). A mirror interference microscope (§2.2.4), where the mirror is formed by a rotating electrode, has been used for this purpose. Rotation is obtained by pivoting the mirror around a point axis by the action of a piezo-electric spacer, in order to produce small movements. The two partial waves from the first biprism are made to impinge on two portions of the mirror separated by 6 $\mu$m and moving in opposite directions with a relative velocity of the order of 60 pm s$^{-1}$. The calculated and measured Doppler frequency shifts agree within 6%. A theoretical treatment of this experiment has been given by Scherzer (1979).

Electron interferometry has been used for teaching purposes: to construct a simple interferometry device (Donati *et al* 1973), to elucidate the statistical nature of the formation of interference fringes (Merli *et al* 1976a, Matteucci and Pozzi 1978) and to clarify the meaning of the vector potential (Woodilla and Schwarz 1971, Matteucci and Pozzi 1978).

### 5.8 *Off-axis electron holography*

Historically, the first attempts to perform electron holography were made by Haine and Mulvey (1952), who used a modified commercial microscope. They managed to obtain a resolution of 2–3 nm with the in-axis (or in-line) technique; further improvements were prevented by various types of instability. This in-line method, which follows the original proposal of Gabor (1948, 1949, 1951), suffers from the inconvenience of the superimposition of twin (or conjugate) images. To overcome this problem, Leith and Upatnieks (1962) devised and applied the off-axis (side-band) holography in light optics. Soon after, Möllenstedt and Wahl (1968) and Wahl (1970c) succeeded in applying this method in electron optics. They

used an electron interferometer equipped with a slit source and an electron biprism. The object consisted of a metal-coated quartz fibre 1 $\mu$m in diameter, which was placed in the path of one of the two partial beams, the other partial beam acting as the reference wave. The resulting interferogram was processed in an optical bench equipped with a laser beam. The reconstructed image showed, in fact, the twin images well separated from each other and from the central spot, which is due to the undeflected beam. This experimental arrangement (essentially a one-dimensional hologram in a direction perpendicular to the biprism wire) is analogous to side-band Fresnel holography, whose resolution is mainly controlled by the spatial coherence.

Similar experiments have been performed in a scanning transmission electron microscope equipped with a 20 kV field emission source (Crewe and Saxon 1971, Saxon 1972a). The resolution in the reconstructed image was about 50 nm and was diffraction-limited by the hologram size. In another paper (Saxon 1972b) the effect of wavefront aberrations, in particular of the coma, on the reconstructed image resolution was investigated.

A different arrangement for off-axis holography is shown in figure 11. The specimen S is placed off axis in the object stage of an electron microscope equipped with a biprism B located

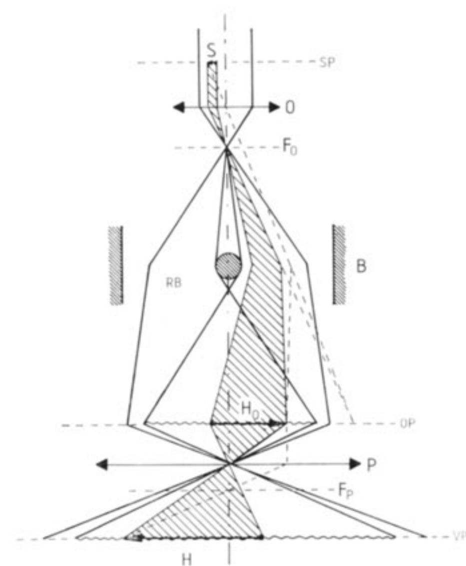


**Figure 11** Schematic arrangement for side-band image electron holography. S, specimen placed off axis; SP, specimen plane; $F_O$, $F_P$, back focal planes of objective O and projector P lenses; B, biprism; RB, reference beam; $H_O$, hologram in the observation plane OP; H, hologram in the viewing plane VP. The broken rays have been used for constructing the image.

behind the back focal plane $F_O$ of the objective lens O. The wave from the object passes on one side of the biprism wire and interferes, in the observation plane OP, with the reference wave RB which has passed on the other side of the wire. If the observation plane is conjugate to the specimen plane SP an off-axis image hologram $H_O$ is produced, otherwise an off-axis Fresnel hologram is formed. Finally, the lens system P provides an enlarged hologram H in the viewing plane VP. This arrangement is essentially the same as that for interference electron microscopy, the only difference being that a large interference field with a high number of fringes (at least above 100 (see figure 12)) is required here. Tomita *et al* (1970, 1972), using this arrangement with a pointed filament and MgO crystal specimens of size ranging from 60 to 100 nm, have estimated the resolution of the reconstructed image to be 2 nm, compared with the expected value of 1 nm. The defocusing distance was 100 $\mu$m and the magnification was $10^4\times$. In the reconstruction bench a spatial frequency filter was used to eliminate the twin image and the straight-through beam.

A conventional transmission electron microscope fitted with a field emission gun (FEG) and with a biprism placed in the diffraction aperture plane was used by Munch (1975). He obtained reconstructed images of Fresnel holograms of MgO crystals (defocusing distance 25 $\mu$m), with a resolution of about 5 nm (laterally) and 10 nm (longitudinally), which is to be compared with the value (0.3 nm) of the capability of the instrument in normal imaging. This fact made Munch turn to the in-line Fraunhofer technique, with which 1 nm diameter gold particles could be detected in the reconstructed real image.

The effect of the spatial coherence of the source on the holograms has been investigated by Menzel *et al* (1973), who conclude that the most suitable technique, in terms of resolution, is that of off-axis image holography (Weingärtner *et al* 1970). These authors estimate a resolution limit of 0.04 nm, set by the combined effects of partial coherence and spherical aberration (the calculations refer to an Elmiskope 1 with $C_S=4$ mm), that is, of one order of magnitude better than that of a conventional electron microscope (Weingärtner *et al* 1969).

The experimental work of Wahl (1973, 1974, 1975) was performed in a small defocusing range, from 1–10 $\mu$m, close to that of side-band image holography. A conventional microscope, fitted with a point filament, an adjustable biprism holder and an image intensifier were used. The illumination divergence was $10^{-5}$ rad and the magnification was $10^4\times$. The reconstructed images were obtained with different light-optics defocus and it was shown that the speckle effect, typical of reconstructed images, could be reduced by using multiple

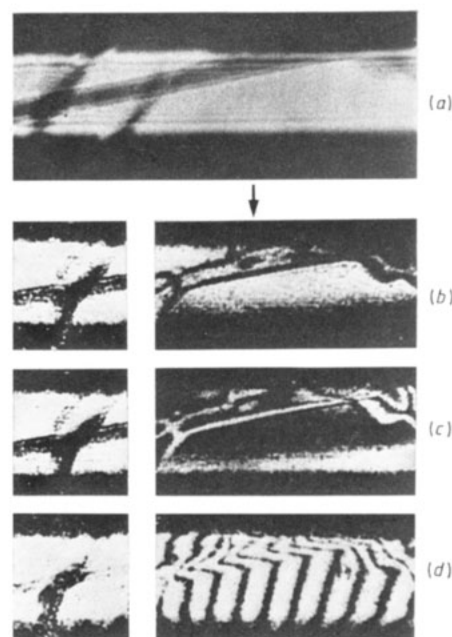


**Figure 12** (*a*) Image plane hologram of ZnO needles. The diffraction fringes visible in (*a*) modulate a much finer interference fringe system (formed by more than 100 fringes) not visible because of the low magnification. (*b*), (*c*) and (*d*) are image reconstructions with (RHS) and without (LHS) an additional reference plane wave. See text for details. The interference field width is 80 nm.

exposures with different aperture diameters in the optical bench. Moreover, Wahl has pointed out the possibility of separating in an optical bench the phase and amplitude terms of the object wavefunction by interference between the optically reconstructed wave and a plane wave (holographic interferometry). A typical example is presented in figure 12, which includes (*a*) an off-axis image hologram of ZnO needles, (*b*), (*c*) and (*d*) (LHS) its conventional reconstructions, and (*b*), (*c*) and (*d*) (RHS), the corresponding holographic interferograms for the detection of the object phase distribution. The latter have been produced by superimposing to the region of interest of hologram (*a*) a plane wave obtained from a portion of the same interference fringe system of (*a*), corresponding to a region without a specimen. In (*b*) the maxima of the two aligned interference fringe systems are coincident (bright field), in (*c*) the maxima overlap the minima (dark field) and in (*d*) the two interference fringe systems are slightly misaligned. A system of holographic interference fringes is visible in the reconstructed image; a maximum phase-shift of about $3\pi$ can be measured in the region marked by the arrow, corresponding to the thickest part of the ZnO crystals. This technique was used by Lau and Pozzi (1978) in the qualitative study of magnetic domain walls in a single crystal of nickel.

All the above experimental work is satisfactory on one hand, since it shows the applicability of several holographic methods to electron optics, and is disappointing on the other hand, since the quality of the reconstructed images is inferior to that of conventional images, both for resolution and for the presence of speckle. In addition, the adoption of FEGs, whose brightness and coherence is 2–3 orders of magnitude greater than that of thermo-ionic sources, has not led to the expected improvements. The reason for this failure lies in the fact that stray magnetic fields, high-voltage instabilities and mechanical vibrations increase the effective source size by a factor 10 and simultaneously decrease by the same factor the illumination coherence, as pointed out by Tonomura *et al* (1978, 1979d). These authors have therefore completely redesigned the electron gun (1979b, d) and improved its stability. They were able to obtain electron interferograms with a biprism, in the absence

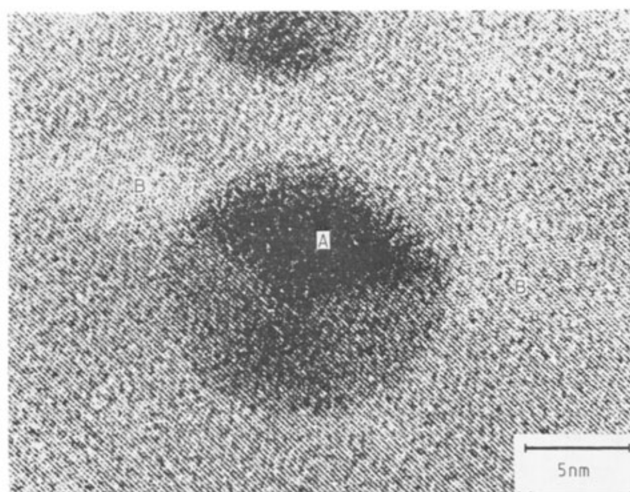


**Figure 13** In-focus, high-resolution, image hologram of an evaporated gold particle, taken with an interference electron microscope equipped with a field emission gun operating at 70 kV. Because of the spherical aberration of the objective lens, the Bragg-reflected images (B) from {111} planes are formed outside the direct image (A). (Courtesy of Tonomura *et al* (1979c), and of the Japanese Journal of Applied Physics.)

of a specimen, containing over 3000 fringes. In addition, reconstructed images of gold particles show lattice fringes of 0.24 nm spacing, which is very close to the resolution limit of the microscope when used for conventional lattice fringe imaging; it should be stressed that the quality of the reconstructed images has been improved and is comparable with that of conventional TEM images. In addition, the information is complete, i.e. amplitude and phase are recorded, as shown by the application of holographic interferometry to the reconstructed image by means of a Mach–Zehnder optical interferometer (Tonomura *et al* 1979a) implemented with phase-difference amplification (Endo *et al* 1979). Moreover, electron microdiffraction patterns from selected specimen areas of lateral dimensions down to 3 nm can be obtained once the electron hologram has been recorded (Tonomura and Matsuda 1980).

The next foreseeable step was the attempt to put into practice Gabor's idea of correcting the spherical aberration in high-resolution images (Tonomura *et al* 1979c). Evaporated fine particles of gold ($\sim 5$ nm diameter) were imaged using the direct beam and two (111) Bragg spots. Owing to the presence of the spherical aberration ($C_s = 1.7$ mm), the image taken at the exact focus is split into three parts: the transmitted image A and the two images B formed by the diffracted beams (figure 13). The latter show a system of fringes, due to interference with the reference beam, which is not visible in conventional microscopes for the low spatial coherence.

Image-plane holograms of these particles were taken at a magnification of $140\,000\times$ (equal to the ratio between the wavelength of the He–Ne laser light used for reconstruction and that of 70 kV electrons) and processed in an optical bench fitted with correction lenses. The reconstructed image can therefore be corrected for spherical aberration until the diffracted images coincide with the transmitted one, and lattice fringes are visible inside it. Half-spacing fringes ($\frac{1}{2}d_{111} = 0.12$ nm) have been observed.

These results are very encouraging, but unfortunately not many microscopes in the world can meet this standard at present.

Electron holographic methods have been reviewed recently by Hawkes (1978), as part of an article on partial coherence, with a very comprehensive list of references, by Zeitler (1979), by Rogers (1980) and by Wade (1980), who gives a detailed and updated account of the whole subject.

## 6 Conclusions

A large amount of experimental work has been performed on the development of different types of interferometry device. The ingenuity of the researchers has succeeded in producing almost all the electron optics counterparts of light optics interferometers. The electrostatic biprism (analogue of the Fresnel biprism in light optics) emerges as by far the most simple, versatile and therefore most used interferometry device. In fact, all practical applications of electron interferometry are based on the biprism. Its working principles have been analysed both experimentally and theoretically, and a satisfactory knowledge of its properties is available.

The use of electron interferometers is nowadays restricted to one or two laboratories; on the other hand, there is a spreading tendency to adapt conventional electron microscopes for work in interference electron microscopy.

The applications of electron interferometry range from inner and contact potential measurements to the detection of small changes of magnetic flux, from the evaluation of fine surface rugosities and specimen thickness to the demonstration of basic properties of the electron waves, from measurements of source coherence to off-axis electron holography. Particular mention is due to the results obtained in the study of fluxons

in superconductors by electron interferometry; recent work on line-of-force mapping in Co crystals opens the possibility of soon being able to produce similar maps for superconducting materials and to solve the old problem of the application of electron microscopy to superconductivity (Hawkes and Valdrè 1977). Further applications of electron interferometry are foreseen in the fields of free-electron lasers, where a continuously tunable optical radiation should be obtained through the production of beats of electron waves in controlled conditions in a biprism interferometer with one split beam periodically accelerated and decelerated (Möllenstedt and Lichte 1979, Schwarz 1979).

A continuous, systematic work has been carried out over the past 25 years by the Tübingen group, the most active in this field, and, in the past, by the Toulouse group. Their work aimed, to a great extent, to confirm the equivalence of the de Broglie electron wavelength to the wavelength of light. The investigations performed closely resemble the work done by Hertz and Righi at the turn of the century, following Maxwell's theoretical results, to prove the occurrence of the well established properties of light for electromagnetic waves. The short electron wavelength has made the task difficult; however, the results can be considered satisfactory, even if the agreement between theory and experiment is quantitative only to a first approximation.

A revival of interest in interference electron microscopy has recently occurred in France, Italy, the United States and particularly in Japan, as well as in Germany, stimulated by the prospects offered by its application to holography. It is, in fact, mainly in this field that interference microscopy is believed to play an important role in the future. The results obtained by Tonomura and collaborators (1979, 1980) in reconstructing and correcting images show a resolution very close to the values reached with standard imaging techniques in the best commercial electron microscopes. This fact is very encouraging in the field of three-dimensional microscopy and in the study of specimens susceptible to irradiation damage, since a single hologram taken with an exposure time of a few seconds contains all the required information (amplitude and phase) for reconstructing an image, which can be corrected in an optical bench for spherical aberration and for defocus, and processed by optical techniques (§5.8). The electron microscope, where the hologram is produced, will be just the first step in a sequence of operations for extracting information from the specimen. There is no doubt that to achieve this task, in the future we will assist in the development of field emission sources which will be highly mechanically and electrically stable and of higher coherence. These will be mounted in electron microscopes which have been carefully protected against mechanical vibration and stray magnetic fields. The development of linear field emission sources might also be forecast since it seems that the brightness requirements for high-resolution work cannot be entirely fulfilled by the present field emission guns.

Finally, may we express the hope that this article will not only indicate the progress that has been made in studying the problem of electron interferometry, but will also stimulate interest in its applications and in the many problems which remain.

**Acknowledgments**
We wish to thank Professor G Möllenstedt for kindly providing figures 7, 8 and 12, Professor H Niedrig for figure 9 and Dr A Tonomura for figure 13.

**References†**

Anaskin I F and Stoyanova I G 1967 Three-beam interference of electrons by means of an electrostatic prism *Dokl. Akad. Nauk SSSR* **174** 56 (transl *Sov. Phys.–Dokl.* **12** 447–50)

Anaskin I F and Stoyanova I G 1968a The phase of an electron wave scattered over a semiplane *Radio Eng. Electron. Phys.* **13** 1104–10

Anaskin I F and Stoyanova I G 1968b Concerning the determination of the mean internal potential in an electron interference microscope *Sov. Phys.–JETP* **27** 904–5

Anaskin I F and Stoyanova I G 1968c Determination of phase of scattered electron wave Rome vol. 1 pp 147–8

Anaskin I F and Stoyanova I G 1968d Multi-beam interference of the electrons by the splitting of wave front Rome vol. 1 pp 149–50

Anaskin I F and Stoyanova I G 1968e Investigation of three-beam electron interference obtained by the use of an electrostatic prism *Radio Eng. Electron. Phys.* **13** 895–902

Anaskin I F and Stoyanova I G 1968f Quality of the interference pattern in an electron beam interferometer *Radio Eng. Electron. Phys.* **13** 789–94

Anaskin I F, Kuminov E S and Stoyanova I G 1968a Interference of electrons on the edge of a thin charged film *JETP Lett.* **7** 61–3

Anaskin I F, Stoyanova I G and Chyapas A F 1966 An electron interference microscope and electron interferometer based on the UEMV-100 electron microscope *Bull. Acad. Sci. USSR, Phys. Ser.* **30** 793–6

Anaskin I F, Stoyanova I G and Shpagina M D 1968b Multibeam interference of electrons achieved by splitting the electron wave front *Bull. Acad. Sci. USSR, Phys. Ser.* **32** 941–6

Bayh W 1962 Messung der kontinuierlichen Phasenschiebung von Elektronenwellen im kraftfeldfreien Raum durch das magnetische Vektorpotential einer Wolfram-Wendel *Z. Phys.* **169** 492–510

Berger H, Kulyupin Yu A, Nepijko S A, Obuchov I A and Shamonya V G 1980 Mean inner potential of bismuth *Z. Phys.* B **37** 23–6

Berndt H and Doll R 1976 Eine Methode zur direkten Phasenbestimmung in elektronenoptischen Beugungsbildern *Optik* **46** 309–32

Berndt H and Doll R 1978 Elektroneninterferenzen zur direkten Phasenbestimmung in elektronenoptischen Beugungsbildern *Optik* **51** 93–6

† In order to avoid continual repetition, the volumes of abstracts of the International and European Congresses on Electron Microscopy are referred to simply by venue: London 1954 (ed. R Ross, London: Royal Microscopical Society), Berlin 1958 (ed. G Möllenstedt, H Niehrs and E Ruska, Berlin: Springer 1960), Rome 1968 (ed. D Bocciarelli, Rome: Tipografia Poliglotta Vaticana), Grenoble 1970 (ed. P Favard, Paris: Société Française de Microscopie Electronique), Canberra 1974 (ed. J V Sanders and D J Goodchild, Canberra: Australian Academy of Sciences), Jerusalem 1976 (ed. D G Brandon, Jerusalem: Tal) and Toronto 1978 (ed. J M Sturgess, Toronto: Microscopical Society of Canada).

Boersch H, Hamisch H and Grohmann K 1962a Experimenteller Nachweis der Phasenverschiebung von Elektronenwellen durch das magnetische Vektorpotential. II *Z. Phys.* **169** 263–72

Boersch H, Hamisch H, Grohmann K and Wohlleben D 1961 Experimenteller Nachweis der Phasenschiebung von Elektronenwellen durch das magnetische Vektorpotential *Z. Phys.* **165** 79–93

Boersch H, Hamisch H, Wohlleben D and Grohmann K 1960 Antiparallele Weissche Bereiche als Biprisma für Elektroneninterferenzen *Z. Phys.* **159** 397–404

Boersch H, Hamisch H, Wohlleben D and Grohmann K 1962b Antiparallele Weissche Bereiche als Biprisma für Elektroneninterferenzen II *Z. Phys.* **167** 72–82

Boersch H and Lischke B 1970a Direkte Beobachtung einzelner magnetischer Flussquanten in supraleitenden Hohlzylindern. I *Z. Phys.* **237** 449–68

Boersch H and Lischke B 1970b Electron interferometric measurements of quantized magnetic flux trapped in superconducting tubes Grenoble vol. 1 pp 69–70

Boersch H, Lischke B, Rodewald W and Söllig H 1974b Magnetic flux-line-pinning in superconducting thin films by decoration microscopy and vortex-microscopy Canberra vol. 1 pp 636–7

Boersch H, Lischke B and Söllig H 1974a Dynamics of single flux lines in superconducting films by vortex microscopy experiments *Phys. Status Solidi* b **61** 215–22

Bonse U and Graeff W 1977 X-ray and neutron interferometry in *X-Ray Optics* ed. H J Queisser (Berlin: Springer) pp 93–143

Braun K-J 1972 Untersuchung der Kohärenzeigenschaften von Elektronenwellen mit dem Elektroneninterferometer *Diplomarbeit* University of Tübingen, Germany

Brünger W 1968 Feldemissionskathode zur kohärenten Beleuchtung des Elektronen-Biprismas *Naturwissenschaften* **55** 295–6

Brünger W 1971 Ultrahochvakuum-Interferometer zur Messung von Kontaktpotentialdifferenzen mit feldemittierten Elektronen *PhD Thesis* University of Tübingen, Germany

Brünger W 1972 Elektroneninterferometer mit Feldemissionskathode zur Messung von Kontaktpotentialdifferenzen im Ultrahochvakuum *Z. Phys.* **250** 263–72

Brünger W and Klein M 1977 Contact potential difference between Au and Ag measured by electron interferometry *Surface Sci.* **62** 317–20

Buhl R 1958 Elektronen-Interferenz-Mikroskopie Berlin vol. 1 pp 233–4

Buhl R 1959 Interferenzmikroskopie mit Elektronenwellen *Z. Phys.* **155** 395–412

Buhl R 1961a Elektronen-Dreistrahlinterferenzen mit elektrostatischen Biprismen *Naturwissenschaften* **48** 298–9

Buhl R 1961b Verfahren zur Kompensation von magnetischen Wechselfeldern in Elektronen-Interferometern *Z. Angew. Phys.* **13** 232–5

Burge R E, Dainty J C and Thom J 1975 The spatial coherence of electron beams in *Developments in Electron Microscopy and Analysis* ed. J A Venables (London: Academic) pp 221–4

Burge R E, Dainty J C and Thom J 1976 Coherence of electron beams Jerusalem vol. 1 pp 256–8

Buxton B F, Rackham G M and Steeds J W 1978 The dynamical theory of a double crystal electron interferometer Toronto vol. 1 pp 188–9

Chambers R G 1960 Shift of an electron interference pattern by enclosed magnetic flux *Phys. Rev. Lett.* **5** 3–5

Crewe A V and Saxon J 1970 Interference experiments with a field emission source *Proc. 28th A. EMSA Meeting, Houston* ed. C J Arceneaux (Baton Rouge: Claitor) pp 534–5

Crewe A V and Saxon J 1971 Electron holography and the correction of spherical aberration *Proc. 29th A. EMSA Meeting, Boston* ed. C J Arceneaux (Baton Rouge: Claitor) pp 12–3

Castaing R and Henry L 1964 Filtrage magnétique des vitesses en microscopie électronique *J. Microscopie* **3** 133–51

Darlington E H and Valdrè U 1975 Imaging of weak Lorentz objects (p–n junctions) by high voltage Fresnel TEM and STEM *J. Phys. E: Sci. Instrum.* **8** 321–4

Donati O, Missiroli G F and Pozzi G 1973 An experiment on electron interference *Am. J. Phys.* **41** 639–44

Dowell W C T 1977 Electron interference in shadow microscopy *Optik* **47** 195–204

Dowell W C T and Goodman P 1973 Image formation and contrast from the convergent electron beam *Phil. Mag.* **28** 471–3

Drahoš V and Delong A 1963 Adaptation of a transmission electron microscope for interference electron microscopy *Česk. Čas. Fys.* A **13** 278–86

Drahoš V and Delong A 1964 The source width and its influence on interference phenomena in a Fresnel electron bi-prism *Opt. Acta* **11** 173–81

Düker H 1955 Lichtstarke Interferenzen mit einem Biprisma für Elektronenwellen *Z. Naturf.* **10** a 256–7

Durand M, Faget J, Ferre J and Fert C 1958 Mesure interférométrique du potentiel interne du graphite *C.R. Acad. Sci., Paris* **247** 590–3

Ehrenberg W and Siday R E 1949 The refractive index in electron optics and the principles of dynamics *Proc. Phys. Soc.* **62** 8–21

Endo J, Matsuda T and Tonomura A 1979 Interference electron microscopy by means of holography *Japan. J. Appl. Phys.* **18** 2291–4

Faget J 1961 Interférences des ondes électroniques: application a une méthode de microscopie électronique interférentielle *Revue Opt.* **40** 347–81

Faget J, Ferré J and Fert C 1958 Le biprisme de Fresnel en optique électronique: influence de la largeur de la source; effet d'une tension périodique appliquée sur le fil du biprisme
*C.R. Acad. Sci., Paris* **246** 1404–7

Faget J and Fert C 1956 Franges de diffraction et d'interférences en optique électronique: diffraction de Fresnel, trous d'Young, biprisme de Fresnel
*C.R. Acad. Sci., Paris* **243** 2028–9

Faget J and Fert C 1957a Microscopie interférentielle et mesure de la différence de phase introduite par une lame en optique électronique
*C.R. Acad. Sci., Paris* **244** 2368–71

Faget J and Fert C 1957b Diffraction et interférences en optique électronique
*Cah. Phys.* **83** 285–96

Feltynowski A 1963 Beobachtung von Elektronen-Biprisma-Interferenzen im Elmiskop
*Z. Angew. Phys.* **15** 312–5

Fert C 1961 Interférences, diffraction en optique électronique et leurs applications à la microscopie in *Traité de microscopie électronique* vol. 1 (Paris: Hermann) pp 234–90

Fert C 1962 The conditions of image-formation in electron optics. Electron microscopy with coherent and incoherent illumination
*J. Electron Microsc.* **11** 1–9

Fert C, Faget J, Fagot M and Ferré J 1962 Un microscope électronique interférentiel
*J. Microscopie* **1** 1–12

Fischer D and Lischke B 1967 Biprismainterferenzen mit langsamen Elektronen
*Z. Phys.* **245** 458–64

Fowler H A, Marton L, Simpson J A and Suddeth J A 1961 Electron interferometer studies of iron whiskers
*J. Appl. Phys.* **32** 1153–5

Françon M 1956 Interférences, Diffraction et Polarisation p 185 in *Handb. Phys.* vol. 24 *Grundlagen der Optik* ed. S Flügge (Berlin: Springer) pp 171–460

Frank J 1976 Determination of source size and energy spread from electron micrographs using the method of Young's fringes
*Optik* **44** 379–91

Frank J, McFarlane S C and Downing K H 1978/9 A note on the effect of illumination aperture and defocus spread in brightfield electron microscopy
*Optik* **52** 49–60

Gabor D 1948 A new microscopic principle
*Nature* **161** 777–8

Gabor D 1949 Microscopy by reconstructed wave-fronts
*Proc. R. Soc.* A **197** 454–87

Gabor D 1951 Microscopy by reconstructed wave fronts: II
*Proc. R. Soc.* B **64** 449–69

Gabor D 1956 Theory of electron interference experiments
*Rev. Mod. Phys.* **28** 260–76

Gesztesy F and Pittner L 1978a Electrons in logarithmic potentials I. Solution of the Schrödinger equation
*J. Phys. A: Math. Gen.* **11** 679–86

Gesztesy F and Pittner L 1978b Electrons in logarithmic potentials II. Solution of the Dirac equation
*J. Phys. A: Math. Gen.* **11** 687–95

Gesztesy F and Pittner L 1978c Diffraction of non-relativistic electron waves by a cylindrical capacitor
*UNI Graz UTP 04/78* pp 1–30

Gesztesy F and Pittner L 1978d Diffraction of relativistic electron waves by a cylindrical capacitor
*UNI Graz UTP 05/78* pp 1–18

Glaser W 1952 *Grundlagen der Elektronenoptik* (Wien: Springer)

Glaser W 1956 Elektronen und Ionen optik
in *Handb. Phys.* vol. 33 ed. S Flügge (Berlin: Springer) pp 123–395

Haine M E and Mulvey T 1952 The formation of the diffraction image with electrons in the Gabor diffraction microscope
*J. Opt. Soc. Am.* **42** 763–73

Hasselbach F 1979 Ein kleines UHV Biprisma-Elektronen-Interferometer für 2 keV-Elektronen
*19 Tagung für Elektronenmikroskopie, Tübingen* p 90 (abstracts)

Hawkes P W 1978 Coherence in electron optics
*Adv. Opt. and Electron Microsc.* vol. 7 ed. V E Cosslett and R Barer (London: Academic) pp 101–84

Hawkes P W and Valdrè U 1977 Superconductivity and electron microscopy
*J. Phys. E: Sci. Instrum.* **10** 309–28

Hegerl R and Hoppe W 1970 Dynamische Theorie der Kristallstrukturanalyse durch Elektronenbeugung im inhomogenen Primärstrahlwellenfeld
*Ber. Bunsenges. Physik Chemie* **74** 1148–54

Hibi T 1974 The effect of the coherence of electron beam on contrast of electron image
Canberra vol. 1 pp 208–9

Hibi T and Takahashi S 1963 Electron interference microscope
*J. Electron Microsc.* **12** 129–33

Hibi T and Takahashi S 1969 Relation between coherence of electron beam and contrast of electron image
*Z. Angew. Phys.* **27** 132–8

Hibi T and Takahashi S 1971 Relation between coherence of electron beam and contrast of electron image of biological substance
*J. Electron Microsc.* **20** 17–22

Hibi T and Yada K 1976 Electron interference microscope in *Principles and Techniques of Electron Microscopy; Biological Applications* vol. 6 ed. M A Hayat (Amsterdam: van Nostrand) pp 312–43

Hoffmann H and Jönsson C 1965 Elektroneninterferometrische Bestimmung der mittleren inneren Potentiale von Al, Cu und Ge unter Verwendung eines neuen Präparationsverfahrens
*Z. Phys.* **182** 360–5

Huber E E Jr 1966 The effect of mercury contamination on the work function of gold
*Appl. Phys. Lett.* **8** 169–71

Jakubovics J P 1976 Lorentz microscopy and applications in *Electron Microscopy in Materials Science* ed. E Ruedl and U Valdrè (Luxembourg: Commission of European Communities) part IV pp 1303–404

Jönsson C 1961 Elektroneninterferenzen an mehreren künstlich hergestellten Feinspalten
*Z. Phys.* **161** 454–74

Jönsson C, Brandt D and Hirschi S 1974 Electron diffraction at multiple slits
*Am. J. Phys.* **42** 4–11

Jönsson C, Hoffmann H and Möllenstedt G 1965 Messungen des mittleren inneren Potentials von Beryllium im Elektronen-Interferometer
*Phys. Kond. Mat.* **3** 193–9

Keller M 1958 Biprisma-Interferometer für Elektronenwellen und seine Anwendung zur Messung von inneren Potentialen
Berlin pp 230–2

Keller M 1961a Ein Biprisma-Interferometer für Elektronenwellen und seine Anwendung
*Z. Phys.* **164** 274–91

Keller M 1961b Elektronen-Zweistrahlinterferenzen mit hohem Gangunterschied
*Z. Phys.* **164** 292–4

Kerschbaumer E 1967 Ein Biprisma-Interferometer für 100 keV Elektronen und seine Anwendung
*Z. Phys.* **201** 200–8

Komrska J 1971 Scalar diffraction theory in electron optics in *Advances in Electronics and Electron Physics* vol. 30 ed. L Marton (New York: Academic) pp 139–234

Komrska J, Drahoš V and Delong A 1964 The application of Fresnel fringes to the determination of the local filament diameter in an electron biprism
*Czech. J. Phys.* B **14** 753–6

Komrska J, Drahoš V and Delong A 1967 Intensity distributions in electron interference phenomena produced by an electrostatic bi-prism
*Opt. Acta* **14** 147–67

Komrska J and Lenc M 1970 The wave mechanical interpretation of the interference phenomena produced by an electrostatic biprism
Grenoble vol. 1 pp 67–8

Komrska J and Vlachová B 1973 Justification of the model for electron interference produced by an electrostatic biprism
*Opt. Acta* **20** 207–15

Krimmel E 1960 Kohärente Teilung eines Elektronenstrahls durch Magnetfelder
*Z. Phys.* **158** 35–8

Krimmel E 1961 Elektronen-Interferenzen in der Umgebung der Brennlinie einer magnetischen Quadrupollinse
*Z. Phys.* **163** 339–55

Krimmel E, Möllenstedt G and Rothemund W 1964 Measurement of contact potential differences by electron interferometry
*Appl. Phys. Lett.* **5** 209–10

Kulyupin Yu A, Nepijko S A, Sedov N N and Shamonya V G 1978/79 Use of interference microscopy to measure electric field distributions
*Optik* **52** 101–9

Kunath W 1978 Phase determination from superposed diffraction patterns
Toronto vol. 1 pp 556–7

Kurz D 1979 Untersuchungen an einen Elektronenstrahlerzeugungssystem mit Feldemissionskathode
*PhD Thesis* University of Tübingen, Germany

Langbein W 1958 Elektroneninterferometrische Messung des inneren Potentials von Kohlenstoff-Folien
*Naturwissenschaften* **45** 510–1

Lau B and Pozzi G 1978 Off-axis electron micro-holography of magnetic domain walls
*Optik* **51** 287–96

Leith E N and Upatnieks J 1962 Reconstructed wavefronts and communication theory
*J. Opt. Soc. Am.* **52** 1123–30

Lenz F A 1972 Path length differences in electron interferometers using mirrors
*Z. Phys.* **249** 462–4

Li M C 1978 A modified Marton-type electron interferometer
*Z. Phys.* B **29** 161–9

Lichte H 1977 Ein Auflicht-Interferenzmikroskop für Elektronenwellen
*PhD Thesis* University of Tübingen, Germany

Lichte H 1979 Ein Elektronen-Auflicht-Interferenzmikroskop zur Präzisionsmessung von Unebenheiten und Potentialunterschieden auf Oberflächen
*PTB Mitteilungen* **89** 229–36

Lichte H and Möllenstedt G 1977 An attempt to investigate the quality of plane surfaces by use of an electron-mirror-interference-microscope
*Proc. 8th Int. Conf. on X-ray Optics and Microanalysis, Boston* (Princeton: Science Press) pp 20–4

Lichte H and Möllenstedt G 1979 Measurement of the roughness of supersmooth surfaces using an electron mirror interference microscope
*J. Phys. E: Sci. Instrum.* **12** 941–4

Lichte H, Möllenstedt G and Wahl H 1972 A Michelson interferometer using electron waves
*Z. Phys.* **249** 456–61

Lischke B 1969 Direct observation of quantized magnetic flux in a superconducting hollow cylinder with an electron interferometer
*Phys. Rev. Lett.* **22** 1366–8

Lischke B 1970a Bestimmung des Fluxoidquants in supraleitenden Hohlzylindern. II
*Z. Phys.* **237** 469–74

Lischke B 1970b Direkte Beobachtung einzelner magnetischer Flussquanten in supraleitenden Hohlzylindern. III
*Z. Phys.* **239** 360–78

Martelli S, Matteucci G and Vittori-Antisari M 1978 Shadow and interference electron microscopy of magnetic domain walls
*Phys. Status Solidi* a **49** K103–7

Marton L 1952 Electron interferometer
*Phys. Rev.* **85** 1057–8

Marton L 1954 Electron interference and phase effects
London pp 272–9

Marton L, Simpson J A and Suddeth J A 1953 Electron beam interferometer
*Phys. Rev.* **90** 490–1

Marton L, Simpson J A and Suddeth J A 1954 An electron interferometer
*Rev. Sci. Instrum.* **25** 1099–104

Matteucci G 1978 On the use of a Wollaston wire in a Möllenstedt-Düker electron biprism
*J. Microsc. Spectrosc. Electron.* **3** 69–71

Matteucci G, Missiroli G F, Merli P G, Pozzi G and Vecchi I 1979b Interference electron microscopy in thin film investigations
*Thin Solid Films* **62** 5–17

Matteucci G and Pozzi G 1978 Two further experiments on electron interference
*Am. J. Phys.* **46** 619–23

Matteucci G and Pozzi G 1980 A 'mixed' type electron interferometer
*Ultramicroscopy* **5** 219–22

Matteucci G, Pozzi G and Vanzi M 1979a Interpretazione d'esperienze d'interferometria elettronica
*Giornale di Fisica* **20** 10–21

Menter J W 1956 The direct study by electron microscopy of crystal lattices and their imperfections
*Proc. R. Soc.* **236** 119–35

Menu C and Evrard D 1971 Interférence en optique électronique. Étude de la visibilité des franges
*C.R. Acad. Sci., Paris* B **273** 309–12

Menzel E, Mirandé W and Weingärtner I 1973
*Fourier-Optik und Holographie* (Wien: Springer)

Merli P G, Missiroli G F and Pozzi G 1974a Electron interferometry with the Elmiskop 101 electron microscope
*J. Phys. E: Sci. Instrum.* **7** 729–32

Merli P G, Missiroli G F and Pozzi G 1974b p–n junction observations by interference electron microscopy
*J. Microscopie* **21** 11–20

Merli P G, Missiroli G F and Pozzi G 1975 Transmission electron microscopy observations of p–n junctions
*Phys. Status Solidi* a **30** 699–711

Merli P G, Missiroli G F and Pozzi G 1976a On the statistical aspect of electron interference phenomena
*Am. J. Phys.* **44** 306–7

Merli P G, Missiroli G F and Pozzi G 1976b Recent results on the observation of the microelectric field of reverse-biased p–n junctions by interference electron microscopy
Jerusalem vol. 1 pp 478–9

Möllenstedt G 1960 Aktuelle probleme der Elektronenmikroskopie
Delft vol. 1 pp 1–17

Möllenstedt G and Bayh W 1961 Elektronen-Biprisma-Interferenzen mit weit getrennten kohärenten Teilbündeln
*Naturwissenschaften* **48** 400

Möllenstedt G and Bayh W 1962 Kontinuierliche Phasenschiebung von Elektronenwellen im kraftfeldfreien Raum durch das magnetische Vektorpotential eines Solenoids
*Physikalische Blätter* **18** 299–305

Möllenstedt G and Buhl R 1957 Ein Elektronen-Interferenze-Mikroskop
*Physikalische Blätter* **13** 357–60

Möllenstedt G and Düker H 1955 Fresnelscher Interferenzversuch mit einem Biprisma für Elektronenwellen
*Naturwissenschaften* **42** 41

Möllenstedt G and Düker H 1956 Beobachtungen und Messungen an Biprisma-Interferenzen mit Elektronenwellen
*Z. Phys.* **145** 377–97

Möllenstedt G and Jönsson C 1959 Elektronen-Mehrfachinterferenzen an regelmässig hergestellten Feinspalten
*Z. Phys.* **155** 472–4

Möllenstedt G and Keller M 1957 Elektroneninterferometrische Messung des inneren Potentials
*Z. Phys.* **148** 34–7

Möllenstedt G and Krimmel E 1963 Herstellung von stromleitenden Wendeln mit extrem kleinen Durchmessern
*Z. Angew. Phys.* **16** 121–4

Möllenstedt G and Lenz F 1962 Some electron interference experiments and their theoretical interpretation
*J. Phys. Soc. Japan* **17** Suppl. B-II 183–6

Möllenstedt G and Lichte H 1978a Young–Fresnelscher Interferenzversuch mit zwei nebeneinander stehenden Spiegeln für Elektronenwellen
*Optik* **51** 423–8

Möllenstedt G and Lichte H 1978b Doppler shift of electron waves
Toronto vol. 1 pp 178–9

Möllenstedt G and Lichte H 1979 Electron interferometry in *Neutron Interferometry* ed. U Bonse and H Rauch (Oxford: Clarendon) pp 363–88

Möllenstedt G, Lichte H, Lau B and Uchikawa Y 1978 Die Anwendung eines fokussierten Laserstrahls zur Heizung der Kathode eines Elektronenstrahl-Erzeugungssystems
*Optik* **51** 417–21

Möllenstedt G and Wahl H 1968 Elektronenholographie und Rekonstruktion mit Laserlicht
*Naturwissenschaften* **55** 340–1

Munch J 1975 Experimental electron holography
*Optik* **43** 79–99

Ohtsuki M and Zeitler E 1977 Young's experiment with electrons
*Ultramicroscopy* **2** 147–8

Pozzi G 1975 Asymptotic approximation of the image wavefunction in interference electron microscopy
*Optik* **42** 97–102

Pozzi G 1980 Asymptotic approximation of the image wavefunction in interference electron microscopy. II Extension to the biprism edges
*Optik* **56** 243–50

Pozzi G and Missiroli G F 1973 Interference electron microscopy of magnetic domains
*J. Microscopie* **18** 103–8

Rackham G M, Loveluck J E and Steeds J W 1977 A double-crystal electron interferometer in *Electron Diffraction 1927–1977* ed. P J Dobson, J B Pendry and C J Humphreys (London, Bristol: The Institute of Physics) pp 435–40

Rodewald W 1977 Electron-optical observation of magnetic flux quanta in superconductors by decoration and vortex microscopy
*Opt. Acta* **24** 665–77

Rogers J 1980 Electron holography in *Imaging Processes and Coherence in Physics* ed. M Schlenket, M Fink, J P Goedgebuer, C Malgrange, J Ch Vlénot and R H Wade (Berlin: Springer) pp 365–70

Saxon G 1972a Division of wavefront side-band Fresnel holography with electrons
*Optik* **35** 195–210

Saxon G 1972b The compensation of magnetic lens wavefront aberrations in side-band holography with electrons
*Optik* **35** 359–75

Schaal G 1971 Ein Biprismainterferometer für 300 keV-Elektronen
*Z. Phys.* **241** 65–81

Schaal G, Jönsson C and Krimmel E F 1966/7 Weitgetrennte kohärente Elektronen-Wellenzüge und Messung des Magnetflusses $\varphi_0 = h/e$
*Optik* **24** 529–38

Scherzer O 1979 Der elektronenoptische Doppler-Effekt
*Optik* **54** 315–23

Schiebel B 1979 Elektroneninterferometrische Bestimmung des mittleren inneren Potentials von epitaktisch aufgestäubten Metallschichten
*19 Tagung für Elektronenmikroskopie, Tübingen* p 90 (abstracts)

Schwarz H 1979 Are 'beats' of electron waves at optical frequencies a potential for free-electron lasers?
*Phys. Rev. Lett.* **42** 1141–4

Septier A 1959 Bipartition d'un faisceau de particules par un biprisme électrostatique
*C.R. Acad. Sci., Paris* **249** 662–4

Simpson J A 1954 The theory of the three-crystal electron interferometer
*Rev. Sci. Instrum.* **25** 1105–9

Simpson J A 1956 Electron interference experiments
*Rev. Mod. Phys.* **28** 254–60

Söllig H 1974 Vortex-Mikroskopie an Dünnschicht-Supraleitern
*PhD Thesis* University of Berlin

Sonier F 1968 Application d'une cathode à pointe à la réalisation d'un interféromètre électronique à lentilles magnétiques
*C.R. Acad. Sci., Paris* B **267** 187–90

Sonier F 1970 Détermination de la valeur du potentiel interne de MgO en microscopie interférentielle
*C.R. Acad. Sci., Paris* B **270** 1536–9

Sonier F 1971 Microscopie électronique interférentielle
*J. Microscopie* **12** 17–32

Speidel R and Kurz D 1977 Richtstrahlwertmessungen an einem Strahlerzeugungssystem mit Feldemissionskathode
*Optik* **49** 173–85

Tomita H, Matsuda T and Komoda T 1970 Electron microholography by two-beam method
*Japan. J. Appl. Phys.* **9** 719

Tomita H, Matsuda T and Komoda T 1972 Off-axis electron microholography
*Japan. J. Appl. Phys.* **11** 143–9

Tomita H and Savelli M 1968 Mesure du potentiel interne de MgO par microscopie interférentielle
*C.R. Acad. Sci., Paris* B **267** 580–3

Tonomura A 1972 The electron interference method for magnetization measurement of thin films
*Japan. J. Appl. Phys.* **11** 493–502

Tonomura A, Endo J and Matsuda T 1979a An application of electron holography to interference microscopy
*Optik* **53** 143–6

Tonomura A and Matsuda T 1980 A new method for micro-area electron diffraction by electron holography
*Japan. J. Appl. Phys.* **19** L97–100

Tonomura A, Matsuda T and Endo J 1979b High resolution electron holography with field emission electron microscope
*Japan. J. Appl. Phys.* **18** 9–14

Tonomura A, Matsuda T and Endo J 1979c Spherical-aberration correction of an electron lens by holography
*Japan. J. Appl. Phys.* **18** 1373–7

Tonomura A, Matsuda T, Endo J, Arii T and Mihama K 1980 Direct observation of fine structures of magnetic domain walls by electron holography
*Phys. Rev. Lett.* **44** 1430–3

Tonomura A, Matsuda T, Endo J, Todokoro H and Komoda T 1979d Development of a field emission electron microscope
*J. Electron Microsc.* **28** 1–11

Tonomura A, Matsuda T and Komoda T 1978 Off-axis electron holography by field emission electron microscope Toronto vol. 1 pp 224–5

Unwin P N T 1971 Phase contrast and interference microscopy with the electron microscope
*Phil. Trans. R. Soc.* B **261** 95–104

Vittori-Antisari M and Valdrè U 1977 Application of a simple RF sputtering apparatus for cleaning purposes in electron microscopy
*J. Microsc. Spectrosc. Electron.* **2** 1–5

Wade R H 1980 Holographic methods in electron microscopy in *Computer Processing of Electron Microscope Images* ed. P W Hawkes (Berlin: Springer) pp 223–55

Wahl H 1968/9 Zur elektroneninterferometrischen Vermessung des in einem supraleitenden Hohlzylinder eingefrorenen Magnetflusses
*Optik* **28** 417–20

Wahl H 1970a Elektroneninterferometrische Messung von quantisierten Magneteinflüssen in supraleitenden Hohlzylindern. I
*Optik* **30** 508–20

Wahl H 1970b Elektroneninterferometrische Messung von quantisierten Magneteinflüssen in supraleitenden Hohlzylindern. II
*Optik* **30** 577–89

Wahl H 1970c Electron optics with highly coherent electron waves
*Ber. Bunsen-Ges.* **74** 1142–8

Wahl H 1973 Bildebenen-Holographie mit Elektronen in *Höchstauflösung in der Elektronenmikroskopie* ed. G Möllenstedt (Munich: Kontron GMBH) pp 86–113

Wahl H 1974 Experimentelle Ermittlung der komplexen Amplitudentransmission nach Betrag und Phase beliebiger elektronenmikroskopischer Objekte mittels der Off-Axis-Bildebenenholographie
*Optik* **39** 585–8

Wahl H 1975 Bildebenenholographie mit elektronen
*PhD Thesis* University of Tübingen, Germany

Wahl H and Lau B 1979 Theoretische Analyse des Verfahrens, die Feldverteilung in dünnen magnetischen Schichten durch lichtholographische Auswertung elektronen-interferenz-mikroskopischer Aufnahmen zu veranschaulichen
*Optik* **54** 27–36

Weingärtner I, Mirandé W and Menzel E 1969 Enhancement of resolution in electron microscopy by image holography
*Optik* **30** 318–22

Weingärtner I, Mirandé W and Menzel E 1970
Holographie bei Teilkohärenz. III Theorie zur
Bildebenen-Holographie
*Optik* **31** 335–53

Woodilla J and Schwarz H 1971 Experiments verifying the
Aharonov–Bohm effect
*Am. J. Phys.* **39** 111–2

Yada K, Shibata K and Hibi T 1973 A high resolution
electron interference microscope and its application to the
measurement of mean inner potential
*J. Electron Microsc.* **22** 223–30

Zeitler E 1979 Electron holography
*Proc. 37th A. EMSA Meeting, San Antonio* ed. G W Bailey
(Baton Rouge: Claitor) pp 376–9

**Ugo Valdrè** is Professer of Experimental Physics and Head of the Electron Microscopy Laboratory of the Physics Department at the University of Bologna, Italy, where he also holds the Chair of Physics for Natural Sciences.

He is a former President of the Italian Society of Electron Microscopy and is presently Director of the International School of Electron Microscopy of the Centre for Scientific Culture 'Ettore Majorana', Erice, Sicily

He has had connections with the Cavendish Laboratory, University of Cambridge since 1960 and is currently responsible for the Italian side of a three year British–Italian collaboration sponsored by the Science Research Council (GB) and Consiglio Nazionale Richerche (I).

A member of the Editorial Board of *J. Phys. E: Sci. Instrum.* from 1973–6, he then served on the Advisory Panel for the journal from 1977–80.

An author of over 100 research papers and author/editor of eight volumes on Electron Microscopy and Physics, Professor Valdrè holds several international patents and a gold medal from the Bavarian Government (West Germany) for outstanding technological achievements in connection with collaborative work with Siemens AG.